

Jean-Pierre Gattuso,

We are pleased to resubmit our manuscript with minor revisions made. In this document we detail how we responded to each reviewer suggestion/comment. After, we provide a complete copy of our manuscript with tracked changes. In our responses to reviewers, our responses are in plain text, and are written among italicized text from reviewers. We indicate text from our revised manuscript in bold.

In addition, we now thank Dr. Judith Hauck by name in the Acknowledgements section. We requested and received her permission to be named there through E-mail.

Sincere thanks,

-Brendan and coauthors

.....
Referee #1

*This paper is much improved in the re-submitted version. Shorter, easier to read, and a good use of the heavy armament in the Princeton-GFDL complex. The history of the field is a bit abbreviated, but that would only lengthen the paper. I only have one comment for curiosity. The authors note the strong signals in the Red Sea. I suspect that the Persian Gulf has perhaps stronger riverine signals overlaid due to the significant river input at the northern end, and older but good quality alkalinity data are available (e.g. Brewer, P. G. and D. Dyrssen (1985). *Chemical Oceanography of the Persian Gulf*. Prog. Oceanog., 14, 41-55.) The Persian Gulf influence is small on the oceanic scale, but it may offer an interesting end member for the discussion.*

The data presented in that paper do indeed suggest the Persian Gulf has a similar *Alk** distribution to the Red Sea. We now note as much:

Brewer and Dyrssen (1985) provide seawater chemistry measurements from the neighboring Persian Gulf that suggest strong calcium carbonate formation results in low *Alk there as well ($< -240 \mu\text{mol kg}^{-1}$ along the Trucial Coast).**

.....
Referee #3

The authors have responded to all of the comments I made. They have not been ignored.

¹ Atmospheric and Oceanic Sciences Program, Princeton University, Princeton, NJ, USA

² Geophysical Fluid Dynamics Laboratory, National Oceanic and Atmospheric Administration, P.O. Box 308, Princeton NJ, 08542, USA

Although I do not completely agree with all of their responses to my comments (for instance, a lack of certainty about errors in the Alk values does not in my opinion justify omitting statistical hypothesis testing), I think the most serious and obvious mistakes have been corrected. However, perhaps not surprisingly given the scale of the changes, other errors have now crept in as detailed below. There are also grammatical errors, references to the wrong figures or figures that no longer exist, etc. I recommend that the manuscript needs to be checked through rigorously one more time by the authors before it can be accepted.*

Line 22: The numbers are wrong. 0.5 – 1.6 Gt C y-1 (in Table 3 of Berelson 2007) converts (multiply by 1000, divide by 12 then multiply by 2) to 80-270 TMol alkalinity y-1. The “x 10” should also be removed.

We removed the “x 10” as rightly suggested. However, we didn’t change our numbers because we are using a different estimate from that paper than the one Reviewer 3 supposed. The range pointed out by the reviewer is for overall calcium carbonate production. We are referring to “net calcium carbonate production” or export... which is listed as 0.4 to 1.8 GtC yr⁻¹... in the abstract and in Table 3.

Line 50: “interested calcium” ?

We added “in” between these two words.

Line 105 should be changed to read “...plus the small (in most places) residual variation...” It is negligible across most of the ocean but in fact rather important in several regions.

Added.

Line 203: there is no figure 6d anymore.

We removed this reference.

Line 211: Only Fig 7b is relevant and it only shows the Bay of Bengal.

We changed this to 6b after swapping the order of figures 6 and 7.

Line 223: Fig 7 no longer shows this.

We swapped the order of figures 6 and 7.

Line 231: Fig 8 no longer shows data from the Red Sea.

This now reads “**Fig. 6.**”

Line 238: better to say “abiotic carbonate formation” (I presume that is the intent) because inorganic carbon(ate) is PIC.

We changed “inorganic” to “abiotic” in several places in that section.

.....
Additional Referee...

Review of Carter et al: Processes determining the marine alkalinity and calcium carbonate saturation distributions

Text to editor and authors:

The paper improved a lot, it is much more concise, well readable and the figures are of good quality. I can now follow why this tracer might be a valuable concept. I can recommend this manuscript for publication in BG after a relatively small number of edits, mostly in the abstract and introduction, that the authors can probably clarify quickly.

Judith Hauck

Normal font is text from the manuscript, suggested edits are in bold, and my comments are in italics.

I italicized all the review text and removed bold formatting.

Comments:

Line 19 give reference after carbon uptake (e.g. Orr et al, 2005, Nature)

Done.

L. 20: give definition of OmegaC. This is used later, but never defined. As this is the main topic of the paper, a short introduction to Omega should be given.

Done:

With marine calcite saturation states decreasing due to anthropogenic carbon uptake (Orr et al., 2005), it is important to understand the degree to which carbonate cycling impacts the calcium carbonate saturation state. Carbonate saturation state is a measure of how supersaturated seawater is with respect to a given mineral form of calcium carbonate. It is expressed as the ratio Ω_C between the product of Ca^{2+} and CO_3^{2-} ion concentrations and the calcite thermodynamic equilibrium solubility product. Values of Ω_C greater than one

indicate calcite precipitation is favored thermodynamically over calcite dissolution, and the reverse is true for values less than one.

L. 36: some calculations → specify which ones use gridded data set or which ones bottle data whatever is easier.

We removed all calculations that used bottle data in previous revisions, so this now reads simply:

We use our gridded dataset in our calculations...

L. 80: give reference for empirical ratio (again)

L. 151-53: „In Fig. 5 we provide ... discrete surface Alk^ Figure 5 also provides ... gridded Alk^* „: I can only see one measure of Alk^* on the y-axis – are these discrete samples or gridded data?*

We provide the gridded mean value in writing on the plots themselves. We are now more clear about this:

Figure 5 also indicates a single volume-weighted mean gridded Alk^* for each basin (in writing).

L. 188: $Alk^ = -16.5 \mu\text{mol/kg}$: give number for other regions, too.*

Done:

Mean Alk^* is higher in the Pacific than the Atlantic and Indian, even when neglecting the region north of 40°N as we do for the Atlantic ($Alk^* = -16.5 \mu\text{mol kg}^{-1}$ when omitted vs. $-22.9 \mu\text{mol kg}^{-1}$ for the Atlantic and $-22.2 \mu\text{mol kg}^{-1}$ for the Indian).

L. 200 from here on Figure numbering is erroneous: Figure 4d → Figure 3d

Fixed.

L. 205: $Alk^ \rightarrow AT$. I assume that Gascard et al refer to AT, not Alk^* as you just introduce this concept here.*

We opted to speak more generally in this revision:

Gascard et al. (2004a, b) suggest that waters along the coast of Norway are part of the Norwegian Coastal Current, and originate in the Baltic and North Seas where there are also strong riverine inputs (Thomas et al., 2005).

Switch Figures 6 and 7 as you describe Figure 7 first and then Figure 6

Switched.

L. 242ff: high-magnesium calcite: your hypothesis only works if you can give a reference that high-Mg calcite is less soluble than biogenic aragonite. According to Morse et al 2006 (doi:10.1016/j.gca.2006.08.017) aragonite is more soluble than synthetic high-Mg-calcite, but less soluble than biogenic high-Mg calcite. So, your hypothesis is possible according to Morse et

al if we assume that inorganically precipitated high-Mg calcite in the open ocean behaves rather like a synthetic high-Mg calcite.

We added text to address this line of thought:

Morse et al. (2006) find that synthetic high magnesium calcite—unlike biogenic high magnesium calcite—is less soluble than aragonite, so this substitution is favored thermodynamically if the abiotic mineral forms similarly to the synthetic mineral.

L. 361-363: Don't give results here of another study (which was not published) which are not part of this manuscript:

AT varies substantially in response to freshwater cycling, so Alk trends may be able to be detected sooner and more confidently attributed to changes in calcium carbonate cycling than trends in AT. Preliminary explorations of Earth System Model output suggest time of trend emergence for the alkalinity trends discussed by Ilyina et al. (2009) could be reduced by as much as a factor of 5. → AT varies substantially in response to freshwater cycling, so Alk* trends may be able to be detected sooner and more confidently attributed to changes in calcium carbonate cycling than trends in AT (Ilyina et al. , 2009).*

We followed this suggestion verbatim.

References: add dois where available.

Added dois to 25 references.

Caption Figure 2: „gridded CARINA, PACIFICA and GLODAP bottle data product“ → gridded or bottle data? Or did you make your own gridded product from all the bottle data?

We did, so we try to be more clear about this in the caption:

Global (a) total alkalinity A_T , (b) salinity, (c) Alk^* , and (d) phosphate distributions at the surface (10 m depth surface) from our gridded CARINA, PACIFICA, and GLODAP bottle data product detailed in Supplementary Materials document SA. Areas with exceptionally poor coverage in the data used to produce the gridded product are blacked out.

Technical corrections:

Title and multiple times throughout the manuscript: calcium carbonate saturation → calcium carbonate saturation state

We added “state“ in many places.

*Line 2: composite tracer for the marine system, Alk^**

Added **for the marine system**

L. 4: We estimate that the...

Added **that**

L. 5: 8 → eight

Changed

L.9: We use the Alk* distribution to estimate the variability of the calcite saturation state

Changed as suggested

L. 10: We show that regional

Added **that**

L. 11: calcite saturation state (throughout the manuscript, will not point to any more occurrences, or use Omega after introducing it)

Changed to Omega in several places and added “state“ in many others.

L. 12: The variations in net calcium carbonate cycling revealed by Alk* play a comparatively minor role in determining the calcium carbonate saturation state.

Changed as suggested

L. 20: impacts the calcium carbonate saturation state

Changed as suggested

L. 22: cycling → sources and sinks

Changed as suggested

L. 28: estimate that hydrothermal

Changed as suggested

L. 50: interested in calcium

Changed as suggested

L. 191: smaller Pacific mean net calcium carbonate formation (or larger CaCO₃ dissolution).

We added “formation“ but omitted the parenthetical statement because it is implied by “net.“

L. 201: Figure 3 → Figure 2

We changed figure numbers here and elsewhere

L. 203: Fig. 6d → Fig. 5d

We changed figure numbers here and elsewhere

L. 211: Figure 7 provides Alk* depth sections for both areas. → Figure 7b provides an Alk* depth section for this area. You only introduced one area so far.

Fixed

L. 212: Bay of Bengal (Fig. 7b)

We fixed the figure number after rearranging figures

L. 214: Ganges (Fig. 7a)

We did not separate these two rivers as suggested since they both feed into the Bay of Bengal (6b)

L. 219: largest AT discharge → largest AT concentration

Discharge is correct. The largest A_T concentration I'm aware of is the Daugava, though I'd guess there are larger.

L. 223: Figure 7 → is actually Figure 6, might be 7 again after switching.

Addressed

L. 231: Fig 8 → Fig. 7

Addressed

L. 252: sea ice that Dieckmann

Added **that**

L. 261 and 262: calcium carbonate cycling (and calcite saturation state)

*Alk** can be affected by magnesium carbonate cycling as well, so we didn't think adding "calcium" would be making the statement more correct.

L. 315: cycling as compared to section 4.1 is

Added a variant on this:

The increased importance of freshwater cycling compared to section 4.1 is because freshwater dilutes C_T by more than the equilibrium C_T decreases from A_T dilution, so carbon uptake tends to follow freshwater precipitation and carbon outgassing follows evaporation.

L. 340/1: and to change

Added "to"

L. 568: then and cancel → then cancel

Deleted "and"

In Figure 8: surface calcite saturation → surface calcite saturation state

Changed to “surface Ω_c ”

Table A1 and A3: Line 5 in this table is misleading, Add another line after this line: „Process *i* bold numbers.“ In the upper line write „ $d\Omega_c/dX_j$ “ and then give bold numbers, in the new/lower line write „Process“ and „*i*“ as headers for the columns below

The suggested changed left some blank space, so we added a little bit more (e.g.):

Table A1. $\frac{\partial\Omega_c}{\partial X_j}$ (bold text) and $\frac{\partial X_{j,i}}{\partial R_i}$ (italic text) terms used in Eq. (A5) for atmospherically isolated mean seawater from all ocean depths. These terms are specific to the $j = 7$ (columns) properties we use to calculate Ω_c and $i = 6$ (rows) processes we consider. Units for $\frac{\partial\Omega_c}{\partial X_j}$ are the inverse of the listed X_j units. Units for $\frac{\partial X_{j,i}}{\partial R_i}$ are the X_j units divided by the R_i units

given in Table 1.

<i>Properties</i>	Pressure	Temp	Salinity	Phos.	Silicate	A_T	C_T	
<i>X_j units</i>	db	°C		μmol/kg	μmol/kg	μmol/kg	μmol/kg	
<i>j</i>	1	2	3	4	5	6	7	
Mean seawater values	2235	3.7	34.71	2.15	49.0	2362	2254	
$\frac{\partial\Omega_c}{\partial X_j}$	-0.00028	0.014	-0.011	-0.0085	-0.00012	0.0082	-0.0079	
Process	<i>i</i>	$\frac{\partial X_{1,i}}{\partial R_i}$	$\frac{\partial X_{2,i}}{\partial R_i}$	$\frac{\partial X_{3,i}}{\partial R_i}$	$\frac{\partial X_{4,i}}{\partial R_i}$	$\frac{\partial X_{5,i}}{\partial R_i}$	$\frac{\partial X_{6,i}}{\partial R_i}$	$\frac{\partial X_{7,i}}{\partial R_i}$
Carbonate cycling	1	-	-	-	-	1	0.5	
Org. matter cycling	2	-	-	-	1	-20.16	117	
Freshwater cycling	3	-	-	1	0.062	68	65	
Sinking / shoaling	4	1	0.00010	-	-	-	-	
Warming / cooling	5	-	1	-	-	-	-	
Denit. / nit. fix.	6	-	-	-	-	-1.26	-	

| **Processes determining the marine alkalinity and calcium carbonate saturation state distributions**

Carter, B. R.¹, J. R. Toggweiler², R. M. Key¹, and J. L. Sarmiento¹

Brendan Carter (brcarter@princeton.edu)

J.R. Toggweiler (Robbie.Toggweiler@noaa.gov)

Robert M. Key (key@princeton.edu)

Jorge L. Sarmiento (jls@princeton.edu)

1 Abstract

2 We introduce a composite tracer for the marine system, Alk^* , that has a global
3 distribution primarily determined by $CaCO_3$ precipitation and dissolution. Alk^* is also affected
4 by riverine alkalinity from dissolved terrestrial carbonate minerals. We estimate that the Arctic
5 receives approximately twice the riverine alkalinity per unit area as the Atlantic, and eight times
6 that of the other oceans. Riverine inputs broadly elevate Alk^* in the Arctic surface and
7 particularly near river mouths. Strong net carbonate precipitation results in low Alk^* in
8 subtropical gyres, especially in the Indian and Atlantic Oceans. Upwelling of dissolved $CaCO_3$
9 rich deep water elevates Northern Pacific and Southern Ocean Alk^* . We use the Alk^*
10 distribution to estimate the variability of the calcite saturation state variability resulting from
11 $CaCO_3$ cycling and other processes. We show that regional differences in surface calcite
12 saturation state are due primarily to the effect of temperature differences on CO_2 solubility and,
13 to a lesser extent, differences in freshwater content and air-sea disequilibria. The variations in
14 net calcium carbonate cycling revealed by Alk^* play a comparatively minor role in determining
15 the calcium carbonate saturation state.

16

17 1. Introduction

18 Our goal is to use high-quality total alkalinity (A_T) observations to examine the effects of
19 calcium carbonate cycling on marine A_T and calcium carbonate saturation states. This study is
20 motivated in part by ocean acidification. With marine calcite saturation states decreasing due to
21 anthropogenic carbon uptake (Orr et al., 2005), it is important to understand the degree to which
22 carbonate cycling impacts the calcium carbonate saturation state-calcite saturations.

23 Carbonate saturation state is a measure of how supersaturated seawater is with respect to

24 a given mineral form of calcium carbonate. It is expressed for calcite as the ratio Ω_c between
 25 the product of Ca^{2+} and CO_3^{2-} ion concentrations and the calcite thermodynamic equilibrium
 26 solubility product. Values of Ω_c greater than one indicate calcite precipitation is favored
 27 thermodynamically over calcite dissolution, and the reverse is true for values less than one.

Field Code Changed

Field Code Changed

Field Code Changed

28 Marine calcium carbonate cycling includes both internal and external calcium carbonate
 29 eyelingsources and sinks. Internal cycling refers to net formation of $67\text{-}300 \times 10^6$ Tmoles $A_T \text{ yr}^{-1}$
 30 worth of calcium carbonate (Berelson et al., 2007) in the surface ocean (Berelson et al., 2007)
 31 and net dissolution of most of this calcium carbonate at depth. External marine carbonate
 32 cycling refers to inputs of carbonate minerals dissolved in rivers, sediment pore waters,
 33 hydrothermal vent fluids, and submarine groundwater discharge, and to loss due to biogenic
 34 carbonate mineral burial and authigenic mineralization in sediments. Rivers add 33 Tmoles A_T
 35 yr^{-1} worth of dissolved bicarbonate to the ocean (Cai et al., 2008). Wolery and Sleep (1988)
 36 estimate that hydrothermal vents add an additional 6.6 Tmoles $A_T \text{ yr}^{-1}$, though deVilliers (1998)
 37 argues the hydrothermal contribution may be as high as 30 Tmoles $A_T \text{ yr}^{-1}$. Submarine
 38 groundwater discharge is poorly constrained, but is thought to exceed riverine inputs in some
 39 areas (Moore, 2010).

40 We investigate calcium carbonate cycling using the global A_T distribution in a dataset we
 41 created by merging the PACIFICA (Suzuki et al., 2013), GLODAP, and CARINA discrete data
 42 products (Key et al. 2004; 2010; Velo et al., 2009). We have combined and gridded these data
 43 products using methods detailed in Supplementary Materials document SA. We use our gridded
 44 dataset in some-our calculations to limit sampling biases and to enable us to make volume-
 45 weighted mean property estimates.

46 Dickson (1981) defines total alkalinity as the concentration excess “of proton acceptors

47 formed from weak acids ($pK \leq 4.5$) relative to proton donors (weak bases with $pK > 4.5$)” at a
48 reference temperature, pressure, and ionic strength. A_T can be thought of as a measure of how
49 well buffered seawater is against changes in pH. This operational definition gives A_T (expressed
50 in mol kg^{-1}) several properties that make it an especially useful carbonate system parameter for
51 examining carbonate cycling:

- 52 1. It mixes conservatively,
- 53 2. ... and is therefore diluted and concentrated linearly by evaporation and precipitation.
- 54 3. It responds in predictable ways to calcium carbonate cycling.
- 55 4. ... as well as organic matter formation and remineralization.
- 56 5. It is not changed by air-sea exchange of heat or carbon dioxide.
- 57 6. It is however affected by anaerobic redox reactions (Chen, 2002).

58 | We are primarily interested in calcium carbonate cycling, item 3 in our list. In section 2 of this
59 | paper we therefore define a tracer we call Alk^* that removes the majority of the influences of
60 | organic matter cycling (item 4), freshwater cycling (item 2), and non-sedimentary anaerobic
61 | redox reactions (item 6) while still mixing conservatively, remaining insensitive to gas exchange,
62 | and responding to calcium carbonate cycling. In section 3 we discuss processes that govern the
63 | Alk^* distribution globally, by ocean basin, and regionally. In section 4 we define a metric to
64 | quantify the influence of various processes on the marine calcite saturation state. We use this
65 | metric with our gridded dataset and Alk^* to determine the relative importance of the various
66 | controls on calcite saturation state -in the ocean and at the ocean surface. We summarize our
67 | findings in section 5.

68

69 **2. The Alk^* tracer**

70 In defining Alk^* , we take advantage of the potential alkalinity (Brewer et al., 1975)
 71 concept to remove the majority of the influence of organic matter cycling and denitrification, and
 72 use a specific salinity normalization scheme (Robbins, 2001) to remove the influence of
 73 freshwater cycling. We detail the Alk^* definition and the reasoning behind it in this section.

74 The influence of organic matter cycling on A_T is due primarily to the biologically-driven
 75 marine nitrogen cycle. Nitrate uptake for anaerobic denitrification and the production of amino
 76 acids occurs in a ~1:1 mole ratio with the release of molecules that increase A_T (Chen, 2002).
 77 Similarly, nitrate from fixation of nitrogen gas and remineralization of amino nitrogen is released
 78 in a 1:1 mole ratio with acids that titrate away A_T (Wolf-Gladrow et al., 2007). This observation
 79 led Brewer et al. (1975) to propose the idea of “potential alkalinity” as the sum of A_T and nitrate
 80 with the aim of creating a tracer that responds to the cycling of calcium carbonates without
 81 changing in response to organic matter cycling. Feely et al. (2002) since used a variant that
 82 relies on the empirical relationship between dissolved calcium concentrations, A_T , and nitrate
 83 determined by Kanamori and Ikegami (1982). This variant has the advantage of implicitly
 84 accounting for the A_T changes created by the exchange of numerous other components of marine
 85 organic matter besides nitrate (e.g. sulfate and phosphate). We thus use the ratio found by
 86 Kanamori and Ikegami (1982) to define potential alkalinity (A_p).

$$87 \quad A_p = A_T + 1.26 * [NO_3^-] \quad (1)$$

88 While the empirical Kanamori and Ikegami (1982) empirical ratio of 1.26 may be specific to the
 89 elemental ratios of the North Pacific, Wolf-Gladrow et al. (2007) provide a theoretical derivation
 90 from Redfield ratios and obtain a similar value of 1.36.

91 The sensitivity of the A_T distribution to freshwater cycling is due primarily to the dilution
 92 or concentration of the large background A_T fraction that does not participate in carbonate

93 cycling on timescales of ocean mixing. This background fraction behaves conservatively, so we
 94 call it conservative potential alkalinity (A_p^C) and estimate it directly from salinity as:

$$95 \quad A_p^C \equiv S \frac{\overline{A_p}}{\overline{S}} \quad (2)$$

96 Here, terms with a bar are reference values chosen as the mean value for those properties in the
 97 top 20 meters of the ocean. We obtain a volume-weighted surface $\overline{A_p}$ (2305 $\mu\text{mol kg}^{-1}$) to \overline{S}
 98 (34.71) ratio of 66.40 $\mu\text{mol kg}^{-1}$ from our gridded dataset. The mean surface values are chosen
 99 in an effort to best capture the impact of freshwater cycling where precipitation and evaporation
 100 occur.

101 Robbins (2001) showed that subtracting an estimate of the conservative portion of a
 102 tracer, such as A_p^C , produces a salinity-normalized composite tracer that mixes conservatively.
 103 This scheme also retains the 2:1 change of A_T to dissolved inorganic carbon (C_T) with carbonate
 104 cycling. We follow this approach in our definition of Alk^* . In Supplementary Materials
 105 document SB we estimate this approach removes 97.5% of the influence of freshwater cycling
 106 on potential alkalinity and reduces the influence of freshwater cycling on Alk^* to less than 1% of
 107 the Alk^* variability. In Supplementary Materials document SC we demonstrate that Alk^* mixes
 108 conservatively, and briefly contrast Alk^* to traditionally normalized potential alkalinity which
 109 does not mix conservatively (Jiang et al., 2014).

110 In total, we define Alk^* as the deviation of potential alkalinity from A_p^C ,

$$111 \quad Alk^* \equiv A_p - A_p^C \quad (3)$$

$$\equiv A_p - \frac{\overline{A_p}}{\overline{S}} S \quad (4)$$

$$\equiv A_p - 66.4 \times S \quad (5)$$

112 where Alk^* has the same units as A_T ($\mu\text{mol kg}^{-1}$). The Alk^* distribution is attributable primarily

113 | to carbonate cycling plus the small (in most places) residual variation due to freshwater cycling
 114 | that is not removed by subtracting A_p^C . However, hydrothermal vent fluid and non-
 115 | denitrification anaerobic redox chemistry may substantively affect alkalinity distributions in
 116 | certain marine environments, and Alk^* distributions could not be attributed purely to internal and
 117 | external calcium carbonate cycling in these locations.

118 | Mean global surface Alk^* is zero by definition, and thus Alk^* can have negative as well
 119 | as positive values. For reference, more than 95% of our gridded Alk^* dataset falls between -35
 120 | and $220 \mu\text{mol kg}^{-1}$. Comparing gridded Alk^* to Alk^* from measurements suggests a standard
 121 | disagreement of order $10 \mu\text{mol kg}^{-1}$. We adopt this number as an estimate of standard gridded
 122 | Alk^* error despite noting there are reasons to suspect that this value could be either an
 123 | underestimate (correlated errors) or an overestimate (we are directly comparing instantaneous
 124 | point measurements to estimates for annual averages for a grid cell).

Formatted: Font: Italic

Formatted: Font: Italic

125

126 | 3. Alk^* distributions

127 | We consider Alk^* distributions globally, by ocean basin, and regionally in the context of
 128 | sources and sinks of the tracer both globally and regionally. We pay special attention to riverine
 129 | Alk^* because it is easily identified where it accumulates near river mouths.

130

131 | 3.1 Global distribution of Alk^*

132 | Figure 1 maps surface Alk^* (top 50 m) at the measurement stations. We provide this
 133 | figure to show where we have viable Alk^* estimates and to demonstrate that our gridded data
 134 | product adequately captures the measured Alk^* distribution. Figure 2 maps gridded global
 135 | surface A_T , salinity, Alk^* , and phosphate distributions and masks the regions that are lacking data

136 in Fig. 1.

137 The similarity of the A_T (Fig. 2a) and salinity (Fig. 2b) distributions demonstrates the
138 strong influence of freshwater cycling on the surface marine A_T distribution (see also: Millero et
139 al. 1998, Jiang et al., 2014). The dissimilarity between Alk^* (Fig. 2c) and salinity (Fig. 2b)
140 suggests Alk^* removes the majority of this influence. The phosphate (Fig. 2d) and Alk^* (Fig. 2c)
141 distributions are similar at the surface. They are also similar at depth: Figures 3 and 4 show
142 zonally-averaged gridded depth sections of Alk^* and phosphate. Alk^* and phosphate
143 concentrations are low in the deep Arctic Ocean (Figs. 3d, and 4d), intermediate in the deep
144 Atlantic Ocean (Figs. 3a and 4a), and high in the deep North Pacific (Figs. 3b and 4b) and deep
145 North Indian (Figs. 3c and 4c) Oceans. Alk^* and phosphate distributions are similar because
146 similar processes shape them: the hard and soft tissue pumps transport A_T and phosphate,
147 respectively, from the surface to depth. The “oldest” water therefore has the highest net
148 phosphate and Alk^* accumulation. High surface phosphate and Alk^* in the Southern Ocean and
149 North Pacific in Figs. 2, 3, and 4 are due to upwelled old deep waters.

150 Several qualitative differences between Alk^* and phosphate distributions are visible in
151 Figs. 2c, 2d, 3, and 4. Surface phosphate is low in the Bay of Bengal and high in the Arabian
152 Sea (Fig. 2d), while the opposite is true for Alk^* (Fig. 2c). Also, Alk^* reaches its highest surface
153 concentration in the Arctic (Figs. 2c and 3d) where phosphate is not greatly elevated (Figs. 2d
154 and 4d). These surface differences are due to regional riverine Alk^* inputs (Section 3.3).
155 Another difference is that Alk^* reaches a maximum below 2000 m in all ocean basins except the
156 Arctic, while phosphate maxima are above 2000 m. We attribute the deeper Alk^* maxima to
157 deeper dissolution of calcium carbonates than organic matter remineralization. Finally, Alk^*
158 values are higher in the deep Indian Ocean than in the deep Pacific. This is likely due to elevated

159 biogenic carbonate export along the coast of Africa and in the Arabian Sea (Sarmiento et al.,
160 2002; Honjo et al., 2008).

161

162 3.2 Alk^* by ocean basin

163 In Fig. 5 we provide 2-D color histograms of discrete surface Alk^* and salinity
164 measurements for the five major ocean basins. Figure 5 also ~~provides~~ *indicates a single* volume-
165 weighted mean gridded Alk^* for each basin (*in writing*). We attribute the decrease in Alk^* as
166 salinity increases—especially visible in the low-salinity bins in the Arctic Ocean (Fig. 5d)—to
167 mixing between high- Alk^* low-salinity river water and low- Alk^* high-salinity open ocean water.
168 Net precipitation in the tropics and net evaporation in the subtropics widens the histograms
169 across a range of salinities and alkalinities without affecting Alk^* in Figs. 5a, 5b, and 5c. The
170 Alk^* elevation associated with upwelled water is most visible in Fig. 5e where Upper
171 Circumpolar Deep Water upwelling near the Polar Front results in high-frequency (i.e. warm
172 colored) histogram bins at high- Alk^* . Similarly, the high-frequency Alk^* bins in Fig. 5b with
173 salinity between 32.5 and 33.5 are from the North Pacific Subpolar Gyre, and are due to
174 upwelled old high- Alk^* water (cf. the Si^* tracer in Sarmiento et al. (2004)). River water
175 contributions can be most easily seen in a scattering of low-frequency (cool colored) high- Alk^*
176 and low-salinity bins in the Arctic Ocean.

177 The surface Southern Ocean has the highest Alk^* followed by the Arctic ~~and the~~ Pacific;
178 ~~and the~~ Indian and Atlantic *have similar and low mean Alk^** . The high mean Southern Ocean
179 Alk^* is due to upwelling. The high mean Arctic surface Alk^* is due to riverine input. The
180 Atlantic and the Arctic together receive ~65% of all river water (Dai and Trenberth, 2002). We
181 construct a budget for terrestrial A_T sources to the various surface ocean basins using the

Formatted: Font: Italic

Formatted: Font: Italic

182 following assumptions:

- 183 1. the A_T of 25 large rivers are as given by Cai et al. (2008),
- 184 2. the volume discharge rates of 200 large rivers are as given by Dai and Trenberth
185 (2002),
- 186 3. groundwater and runoff enter each ocean in the same proportion as river water from
187 these 200 rivers,
- 188 4. the A_T of all water types that we do not know from assumption 1. is the $1100 \mu\text{mol}$
189 kg^{-1} global mean value estimated by Cai et al. (2008), and
- 190 5. 40°N is the boundary between the Atlantic and the Arctic and 40°S is the boundary
191 between the Southern and the Atlantic Oceans (based upon the region of elevated
192 surface phosphate in Fig. 2d),

193 Our detailed budget is provided as Supplementary Materials file SD. We estimate 40% of
194 continentally derived A_T enters the Atlantic, 20% enters the Arctic, and 40% enters all remaining
195 ocean basins. These ocean areas represent 17%, 5%, and 78% of the total surface ocean area in
196 our gridded dataset respectively, so the Arctic receives approximately twice as much riverine A_T
197 per unit area as the Atlantic, and 8 times the rest of the world ocean. The Atlantic has the lowest
198 open-ocean surface Alk^* value and ~~the lowest~~ basin mean surface Alk^* despite the large riverine
199 sources. The large riverine A_T input must therefore be more than balanced by strong net calcium
200 carbonate formation. The Indian Ocean has comparably low mean surface Alk^* to the Atlantic,
201 but a smaller riverine source. Mean Alk^* is higher in the Pacific than the Atlantic and Indian,
202 even when neglecting the ~~upwelling~~-region north of 40°N as we do for the Atlantic ($Alk^* = -16.5$
203 $\mu\text{mol kg}^{-1}$ when omitted vs. $-22.9 \mu\text{mol kg}^{-1}$ for the Atlantic and $-22.2 \mu\text{mol kg}^{-1}$ for the
204 Indian). The difference between the Pacific and the other basins is significant when considering

205 the large number of grid cell Alk^* values averaged (> 6000 in the Atlantic), and the small
 206 estimated uncertainty for each value ($\sim 10 \mu\text{mol kg}^{-1}$). Considering the weak Pacific riverine
 207 input, this suggests that, relative to other ocean basins, there are either larger Alk^* inputs from
 208 exchange with other basins and deeper waters or smaller Pacific basin mean net calcium
 209 carbonate formation.

Formatted: Font: Italic

Formatted: Superscript

211 3.3 Riverine Alk^* regionally

212 For river water with negligible salinity, Alk^* equals the potential alkalinity. This
 213 averages around $1100 \mu\text{mol kg}^{-1}$ globally (Cai et al., 2008), but is greater than $3000 \mu\text{mol kg}^{-1}$
 214 for some rivers (Beldowski et al., 2010). Evidence suggests that riverine A_T is increasing due to
 215 human activities (Kaushal et al., 2013).

216 The most visible riverine Alk^* signals are in the Arctic due to the large riverine runoff
 217 into this comparatively small basin and the confinement of this low-density riverine water to the
 218 surface (Jones et al., 2008; Yamamoto-Kawai et al., 2009; Azetsu-Scott et al., 2010). Figure 43d
 219 shows the high Arctic Alk^* plume is confined to the top ~ 200 m. Figure 3-1 shows that these
 220 high Alk^* values extend along the coast of Greenland and through the Labrador Sea. Alk^*
 221 decreases with increasing salinity in this region (Fig. 56d) due to mixing between the fresh high
 222 Alk^* surface Arctic waters and the salty lower Alk^* waters of the surface Atlantic. Gascard et al.
 223 (2004a, b) suggest that ~~high Alk^*~~ waters along the coast of Norway are part of the Norwegian
 224 Coastal Current, and originate in the Baltic and North Seas where there are also strong riverine
 225 inputs (Thomas et al., 2005).

226 Elevated Alk^* can also be seen in the Bay of Bengal with surface values $\sim 100 \mu\text{mol kg}^{-1}$
 227 higher than those in the central Indian Ocean. This bay has two high A_T rivers that join and flow

228 into it, the Brahmaputra ($A_T = 1114 \mu\text{mol kg}^{-1}$) and the Ganges ($A_T = 1966 \mu\text{mol kg}^{-1}$) (Cai et al.,
229 2008). Figure 7-6b provides an Alk^* depth section ~~for this regions for both areas~~. The riverine
230 Alk^* plume can be clearly seen in the top 50 m ~~of the Bay of Bengal~~. No similar increase is seen
231 in the Arabian Sea (Fig. 6a) where the Indus River ($1681 \mu\text{mol kg}^{-1}$) discharges only $\sim 1/10$ th of
232 the combined volume of the Brahmaputra and the Ganges.

233 The Amazon River is the largest single riverine marine A_T source. This river has low A_T
234 ($369 \mu\text{mol kg}^{-1}$ (Cai et al., 2008)), but has the largest water discharge volume of any river,
235 exceeding the second largest—the Congo—by a factor of ~ 5 (Dai and Trenberth, 2002).
236 Consequently, the Amazon discharges approximately 50% more A_T per year than the river with
237 the second largest A_T discharge, the Changjiang (Cai et al., 2008). The Amazon's influence can
238 be seen as a region of abnormally low salinity and A_T in Fig. 2a and b. Despite the high
239 discharge volume, the influence is only barely visible as a region of elevated Alk^* in Fig. 2c due
240 to the comparatively low Amazon Alk^* . However, the influence of the Amazon on Alk^* can be
241 seen in the seasonal Alk^* cycle in the Amazon plume. Figure 7 provides a map of Alk^* for this
242 region scaled to show the influence of this low Alk^* river in the Northern Hemisphere (a) winter
243 and (b) summer months. The higher Alk^* found for summer months is consistent with Amazon
244 discharge and A_T seasonality (Cooley et al., 2007) and Moore et al.'s (1986) radium isotope
245 based finding that Amazon River outflow comprises 20-34% of surface water in this region in
246 July compared to only 5-9% in December.

247

248 3.4 Regional ~~inorganic-abiotic~~ carbonate cycling

249 The Red Sea portion of Fig. 8-6a is strongly depleted in Alk^* , and contains the lowest
250 single Alk^* measurement in our dataset, $-247 \mu\text{mol kg}^{-1}$. The GEOSECS expedition Red Sea

251 alkalinity measurements (Craig and Turekian, 1980) predate alkalinity reference materials
 252 (Dickson et al., 2007), but are supported by more recent measurements (Silverman et al., 2007).
 253 Like Jiang et al. (2014), we attribute low Red Sea Alk^* to exceptionally active calcium carbonate
 254 formation. Brewer and Dyrssen (1985) provide seawater chemistry measurements from the
 255 neighboring Persian Gulf that suggest strong calcium carbonate formation results in low Alk^*
 256 there as well ($< -240 \mu\text{mol kg}^{-1}$ along the Trucial Coast).

257 The Red Sea is one of the only regions where Ω_c ~~calcium carbonate saturation~~ is
 258 sufficiently high for ~~inorganic-abiotic~~ carbonate precipitation to significantly contribute to
 259 overall carbonate precipitation (Milliman et al. 1969; Silverman et al., 2007). Notably,
 260 saturation state remains high at depth in the Red Sea (see Section 4.2). In this region, biogenic
 261 aragonitic corals and pteropod shells are progressively removed with depth in sediments, and
 262 pores left behind are filled in with high-magnesium calcite cement (Gevirtz and Friedman, 1966;
 263 Despite this, carbonate sediments in the modern Red Sea are mostly biogenic aragonitic corals
 264 and pteropod shells (Gevirtz and Friedman, 1966). However, in this region, pores in sediments
 265 are filled in with high magnesium calcite cement (Almogi-Labin et al., 1986). We hypothesize
 266 biogenic carbonates are dissolved by CO_2 from sedimentary organic matter remineralization, as
 267 occurs elsewhere (e.g. Hales and Emerson, 1997; Hales, 2003; Boudreau, 2013), ~~but and~~ that
 268 high deep Red Sea Ω_c ~~calcium carbonate saturation~~ leads to ~~inorganic-abiotic~~ re-calcification in
 269 sediment pores. Morse et al. (2006) find that synthetic high magnesium calcite—unlike biogenic
 270 high magnesium calcite—is less soluble than aragonite, so this substitution is favored
 271 thermodynamically if the abiotic mineral forms similarly to the synthetic mineral.

272 ~~Inorganic-e~~Calcium carbonate has recently been found as metastable ikaite (a hydrated
 273 ~~calcium carbonate~~ mineral with the formula $\text{CaCO}_3 \cdot 6\text{H}_2\text{O}$) in natural sea ice (Dieckmann et al.,

Field Code Changed

Field Code Changed

274 2008). Ikaite cycling provides a competing explanation for the high Arctic surface Alk^* values if
 275 high A_T low-salinity ikaite-rich ice melt becomes separated from low A_T high-salinity rejected
 276 brines. However, riverine A_T inputs better explain the magnitude of the feature: The ~ 5 mg
 277 ikaite L^{-1} sea ice [that](#) Dieckmann et al. (2008) found in the Antarctic could only enrich A_T of the
 278 surface 100 m by $\sim 1 \mu\text{mol kg}^{-1}$ for each meter of ice melted, and Arctic surface 100 m Alk^* is
 279 elevated by $59 \mu\text{mol kg}^{-1}$ relative to the deeper Arctic in our gridded dataset. By contrast, Jones
 280 et al. (2008) estimate a $\sim 5\%$ average riverine end-member contribution to the shallowest 100 m
 281 of this region, which accounts for $\sim 55 \mu\text{mol kg}^{-1}$ Alk^* enrichment. Also, surface Alk^* in the
 282 Southern Ocean—which has sea ice but lacks major rivers—is not similarly elevated relative to
 283 [surface](#) phosphate (Fig. 2) or deep Alk^* (Fig. 3).

284

285 4. Controls on the calcite saturation state

286 The Alk^* tracer provides an opportunity to estimate the impact of carbonate cycling on
 287 Ω_c ~~the calcite saturation~~. In addition to (1) carbonate cycling, Ω_c ~~calcite saturation~~ is affected
 288 by (2) organic matter cycling, (3) freshwater cycling, (4) pressure changes on seawater, (5)
 289 heating and cooling, and (6) A_T changes from nitrogen fixation and denitrification. For each of
 290 these six processes, we estimate the standard deviation of the net influence of the process
 291 globally by considering the standard deviation of a “reference” tracer R_i for the process, “ σ_{R_i} ”,
 292 where R_i is Alk^* for CaCO_3 cycling, phosphate for organic matter cycling, salinity for
 293 freshwater cycling, pressure for pressure changes, temperature for heating and cooling, and N^*
 294 (Gruber and Sarmiento, 1997) for nitrogen fixation and denitrification. We use the standard
 295 deviation of the reference tracer as a measure of the oceanic range of the net influence of the
 296 corresponding process. We measure the impact of this range on Ω_c ~~calcite saturation~~ using a

Field Code Changed

Field Code Changed

Field Code Changed

297 metric M , which we define as:

$$298 \quad M_i = \sigma_{R_i} |S_{R_i}| \quad (6)$$

299 where S_{R_i} is the Ω_c calcite saturation sensitivity to a unit process change in R_i , which we

300 estimate in Appendix A. We are interested in the relative importance I of our 6 processes, so we

301 also calculate the percentage that each metric value estimate contributes to the sum of all 6

302 metric value estimates:

$$303 \quad I_i = 100\% \times \frac{M_i}{\sum_{i=1}^6 M_i} \quad (7)$$

304 We derive and estimate our metric and its uncertainty in Appendix A. We carry out our analysis

305 for the full water column assuming it to be isolated from the atmosphere (section 4.1), and also

306 for just the top 50 m of the water column assuming it to be well-equilibrated with the atmosphere

307 (section 4.2). Finally, we consider how equilibration with an atmosphere with a changing $p\text{CO}_2$

308 alters surface Ω_c calcite saturation.

309

310 *4.1 Process importance in atmospherically-isolated mean seawater from all ocean depths*

311 Our metric M_i is an estimate of the standard deviation of the global distribution of Ω_c

312 resulting from the i th process. Our relative process importance metric I_i is an estimate of the

313 percentage of overall variability of the Ω_c distribution that can be attributed to that process. We

314 provide M and I values for mean seawater from the full water column alongside the R_i , S_{R_i} , and

315 σ_{R_i} values used to estimate them in Table 1. These calculations assume that the seawater is

316 isolated from the atmosphere.

317 Relative process importance estimates I indicate organic matter cycling (48%) is the

Field Code Changed

Formatted: Font: Italic

Field Code Changed

318 dominant process controlling Ω_c ~~calcite saturation~~ for mean seawater. Changing pressure (28%)
 319 is the second most important process, followed by calcium carbonate cycling (17%), temperature
 320 changes (4%), nitrogen fixation and denitrification (1.21%), and freshwater cycling (0.78%).

321

322 4.2 Process importance in well-equilibrated surface seawater

323 In Table 2 we provide M_i values for well-equilibrated seawater in the top 50 m of the
 324 ocean alongside the R_i, σ_R, S_R used to estimate them. These surface seawater M_i values are
 325 calculated assuming the water remains equilibrated with an atmosphere with 400 $\mu\text{atm } p\text{CO}_2$.
 326 We test the validity of this assumption by also estimating M for the observed global $p\text{CO}_2$
 327 variability in the Takahashi et al. (2009) global data product. This test reveals transient air-sea
 328 disequilibria are indeed important for surface ocean Ω_c ~~calcite saturation~~, but only as a
 329 secondary factor when considered globally. Despite this, it is important to recognize that air-sea
 330 equilibration following a process is not instantaneous, and that the S_R value estimates in section
 331 4.1 ~~will~~ may be better for estimating short term changes following fast acting processes such as
 332 spring blooms (e.g. Tynan et al., 2014) or upwelling events (e.g. Feely et al., 1988). We omit the
 333 disequilibrium M value estimate from the denominator of Eq. (7) to allow I values for surface
 334 seawater to be compared to I values from mean seawater globally.

335 Warming and cooling are the dominant processes controlling Ω_c for well-equilibrated
 336 surface seawater (76%). The large increase in M for warming and cooling relative to the value
 337 calculated for mean seawater is due to lower equilibrium C_T at higher temperatures. Freshwater
 338 cycling is the second most important process (13%), followed by carbonate cycling (8%),
 339 organic matter cycling (2%), pressure changes (1%), and denitrification and nitrogen fixation

Field Code Changed

Field Code Changed

340 (0.4%). The increased importance of freshwater cycling [compared to section 4.1](#) is because
 341 freshwater dilutes C_T by more than the equilibrium C_T decreases from A_T dilution, so carbon
 342 uptake tends to follow freshwater precipitation and carbon outgassing follows evaporation.
 343 Carbonate cycling is less important because A_T decreases with carbonate precipitation lead to
 344 lower C_T at equilibrium. Organic matter cycling is much less important because atmospheric re-
 345 equilibration mostly negates the large changes in C_T . Pressure changes are negligible because
 346 we only consider water in the surface 50 m. Our air-sea disequilibrium M estimate suggests
 347 surface disequilibria are comparably important to freshwater cycling for surface Ω_c ~~calcite~~
 348 ~~saturation~~, but substantially less important than temperature changes (this would correspond to
 349 an I value of ~14%).

Field Code Changed

350 The dominance of warming and cooling and freshwater cycling over carbonate cycling is
 351 most evident in the Red Sea where high temperatures (>25 °C) and high salinities (>40) lead to
 352 surface Ω_c ~~calcite saturations~~ exceeding 6 despite extremely low Alk^* (<-200 $\mu\text{mol kg}^{-1}$). The
 353 deep Red Sea is also unusual for having deep water that was warm when it last left contact with
 354 the atmosphere (the Red Sea is >20 °C at >1000 m depth). This provides high initial deep Ω_c
 355 ~~calcite saturation~~ that—combined with decreased influence of pressure changes at higher
 356 temperatures—keeps deep Red Sea $\Omega_c > 3$. Similarly, the lowest surface Ω_c ~~values saturation~~
 357 ~~states~~ are in the Arctic where there are low temperatures, low salinity, and high Alk^* from
 358 riverine inputs. The importance of warming and cooling is also suggested by the correlation
 359 between global surface Ω_c ~~calcite saturation~~ and the surface temperature ($R^2 = 0.96$). These
 360 properties are plotted shown for our gridded dataset in Fig. 8.

Field Code Changed

Field Code Changed

Field Code Changed

Field Code Changed

361

362 5. Conclusions

363 Alk^* isolates the portion of the A_T signal that varies in response to calcium carbonate
 364 cycling and exchanges with terrestrial and sedimentary environments from the portion that varies
 365 in response to freshwater and organic matter cycling. The salinity normalization we use has the
 366 advantage over previous salinity normalizations that it allows our tracer to mix linearly and to
 367 change in a 2:1 ratio with C_T in response to carbonate cycling. We highlight the following
 368 insights from Alk^* :

369 (1) *Alk* distribution*: The Alk^* distribution clearly shows the influence of biological
 370 cycling including such features as the very low Alk^* in the Red Sea due to the high calcium
 371 carbonate precipitation there. We also find evidence of strong riverine A_T sources in the Bay of
 372 Bengal and in the Arctic. We show river inputs likely dominate over the small influences of
 373 ikaite cycling on the Arctic alkalinity distribution.

374 (2) *Influence of calcium carbonate cycling on marine calcite saturation state*: Alk^* allows
 375 us to quantify the net influence of calcium carbonate cycling on marine Ω_c ~~calcite saturation~~.
 376 For well-equilibrated surface waters, carbonate cycling is less influential for Ω_c ~~calcite~~
 377 ~~saturation~~ than gas exchange driven by warming and cooling and freshwater cycling. At depth,
 378 the carbonate cycling signal is smaller than the signal from organic matter cycling and from
 379 pressure changes. Temperature is the dominant control on Ω_c ~~calcite saturation~~ of surface
 380 waters in equilibrium with the atmosphere. This accounts for the low calcite saturation states in
 381 the cold surface of the Arctic and Southern Oceans despite high regional Alk^* , and high Ω_c
 382 ~~calcite saturations~~ in the warm subtropics despite low regional Alk^* .

383 We intend to use Alk^* for two future projects. First, Alk^* is superior to A_T for monitoring

Formatted: Font: Italic

Field Code Changed

Field Code Changed

Field Code Changed

Field Code Changed

384 and modeling changes in marine chemistry resulting from changes in carbonate cycling with
385 ocean acidification. A_T varies substantially in response to freshwater cycling, so Alk^* trends may
386 be able to be detected sooner and more confidently attributed to changes in calcium carbonate
387 cycling than trends in A_T . ~~Preliminary explorations of Earth System Model output suggest time~~
388 ~~of trend emergence for the alkalinity trends discussed by (Ilyina et al. (2009) could be reduced~~
389 ~~by as much as a factor of 5.~~ Secondly, we will estimate global steady state Alk^* distributions
390 using Alk^* sources and sinks from varied biogeochemical ocean circulation models alongside
391 independent water mixing and transport estimates (e.g. Khatiwala et al., 2005; Khatiwala, 2007).
392 We will interpret findings in the context of two hypotheses proposed to explain evidence for
393 calcium carbonate dissolution above the aragonite saturation horizon: (1) that organic matter
394 remineralization creates undersaturated microenvironments that promote carbonate dissolution in
395 portions of the water column which are chemically supersaturated in bulk, and (2) that high-
396 magnesium calcite and other impure minerals allow chemical dissolution above the saturation
397 horizon.

398

399 Acknowledgements

400 We thank Eun Young Kwon for contributions to early versions of this research. We also
401 thank the US National Science Foundation for research support (ANT-1040957), as well as the
402 numerous scientists and crew that contributed to the datasets used in this study. R. Key was
403 supported by CICS grant NA08OAR432052. We also ~~thank Dr. Judith Hauck and three~~
404 ~~anonymous reviewers for their helpful and constructive~~ reviews ~~comments~~.

405

406 References

Formatted: Not Superscript/ Subscript

- 407 Almogi-Labin, A., B. Luz, and J. Duplessy (1986), Quaternary paleo-oceanography, pteropod
408 preservation and stable-isotope record of the Red Sea, *Palaeogeogr., Palaeoclimatol.,*
409 *Palaeoecol.*, 57, 195-211, ~~DOI~~doi: 10.1016/0031-0182(86)90013-1.
- 410 Anderson, L. A. and J. L. Sarmiento (1994), Redfield ratios of remineralization determined by
411 nutrient data analysis, *Global Biogeochem. Cycles*, 8, 65-80, doi: 10.1029/93GB03318.
- 412 Azetsu-Scott, K., A. Clarke, K. Falkner, J. Hamilton, E. P. Jones, C. Lee, B. Petrie, S.
413 Prinsenberg, M. Starr, and P. Yeats (2010), Calcium carbonate saturation states in the waters
414 of the Canadian Arctic Archipelago and the Labrador Sea, *J. Geophys. Res. Oceans*, 115,
415 C11, doi: [10.1029/2009JC005917](https://doi.org/10.1029/2009JC005917).
- 416 Beldowski, J., A. Löffler, B. Schneider, and L. Joensuu (2010), Distribution and biogeochemical
417 control of total CO₂ and total alkalinity in the Baltic Sea, *J. Mar. Sys.*, 81, 252-259.
418 doi:[10.1016/j.jmarsys.2009.12.020](https://doi.org/10.1016/j.jmarsys.2009.12.020).
- 419 Berelson, W. M., W. M. Balch, R. Najjar, R. A. Feely, C. Sabine, and K. Lee (2007), Relating
420 estimates of CaCO₃ production, export, and dissolution in the water column to measurements
421 of CaCO₃ rain into sediment traps and dissolution on the sea floor: A revised global
422 carbonate budget, *Global Biogeochem. Cycles*, 21, GB1024, doi: 10.1029/2006GB002803.
- 423 Boudreau, B. P. (2013), Carbonate dissolution rates at the deep ocean floor, *Geophys. Res. Lett.*,
424 40, 1-5, doi: 10.1029/2012GL054231.
- 425 [Brewer, P. G., and D. Dyrssen \(1985\), Chemical oceanography of the Persian Gulf. *Prog.*](#)
426 [Oceanogr.](#), 14, 41-55, doi:[10.1016/0079-6611\(85\)90004-7](https://doi.org/10.1016/0079-6611(85)90004-7).
- 427 Brewer, P. G., G. T. F. Wong, M. P. Bacon, D. W. Spencer (1975), An oceanic calcium
428 problem? *Earth and Planet. Sci. Lett.*, 26 (1), 81-87, doi: 10.1016/0012-821X(75)90179-X.
- 429 Cai, W.-J. X. Guo, C. A. Chen, M. Dai, L. Zhang, W. Zhai, S. E. Lohrenz, K. Yin, P. J. Harrison,

- 430 Y. Wang (2008), A comparative overview of weathering intensity and HCO_3^- flux in the
431 world's major rivers with emphasis on the Changjiang, Huanghe, Zhujiang (Pearl) and
432 Mississippi Rivers, *Continental Shelf Res.*, 28, 1538-1549, doi:10.1016/j.csr.2007.10.014.
- 433 Chen, C.-T. A. (2002), Shelf-vs. dissolution-generated alkalinity above the chemical lysocline,
434 *Deep Sea Res. II*, 49 (24–25), 5365-5375, doi: 10.1016/S0967-0645(02)00196-0.
- 435 Cooley, S. R., V. J. Coles, A. Subramaniam, and P. P. Yager (2007), Seasonal variations in the
436 Amazon plume-related atmospheric carbon sink, *Global Biogeo. Chem. Cycles.*, 21 (3),
437 GB3014, doi: 10.1029/2006GB002831.
- 438 Craig, H., and K.K. Turekian (1980), The GEOSECS program 1976-1979, *Earth Planet. Sci.*
439 *Lett.*, 49, 263-265, doi: 10.1016/j.bbr.2011.03.031.
- 440 Dai, A. and K. E. Trenberth (2002), Estimates of freshwater discharge from continents: latitudi-
441 nal and seasonal variations, *J. Hydrometeorology*, 3, 660-687,
442 doi: [http://dx.doi.org/10.1175/1525-7541\(2002\)003<0660:EOFDFC>2.0.CO;2](http://dx.doi.org/10.1175/1525-7541(2002)003<0660:EOFDFC>2.0.CO;2).
- 443 Dickson, A.G. (1981), An exact definition of total alkalinity and a procedure for the estimation
444 of alkalinity and total inorganic carbon from titration data, *Deep Sea Res. A*, 28 (6), 609-623,
445 doi: 10.1016/0198-0149(81)90121-7.
- 446 Dickson, A. G. and F. J. Millero (1987), A comparison of the equilibrium constants for the
447 dissociation of carbonic acid in seawater media, *Deep-Sea Res. A*, 34, 1733-1743,
448 doi:10.1016/0198-0149(87)90021-5.
- 449 Dieckmann, G.S., G. Nehrke, S. Papadimitriou, J. Göttlicher, R. Steininger, H. Kennedy, D.
450 Wolf-Gladrow, and D. N. Thomas (2008), Calcium carbonate as ikaite crystals in Antarctic
451 sea ice, *Geophys. Res. Lett.*, 35, L08051, doi:10.1029/2008GL033540.
- 452 Feely, R. A., C. L. Sabine, K. Lee, F. J. Millero, M. F. Lamb, D. Greeley, J. L. Bullister, R. M.

- 453 Key, T. H. Peng, and A. Kozyr (2002), In situ calcium carbonate dissolution in the Pacific
 454 Ocean. *Global Biogeochem. Cycles*, 16, 1144, doi: 10.1029/2002GB001866.
- 455 Feely, R. A., R.H. Byrne, J. G. Acker, P. R. Betzer, C. A. Chen, J. F. Gendron, and M. F. Lamb
 456 (1988), Winter-summer variations of calcite and aragonite saturation in the northeast
 457 Pacific. *Mar. Chem.* 25, 3, 227-241, doi:10.1016/0304-4203(88)90052-7.
- 458 Fofonof, N. P., and R. C. Millard (1983), Algorithms for computations of fundamental properties
 459 of seawater. UNESCO Technical Papers in Marine Science No. 44, 53 pp.
- 460 Gascard, J. C., G. Raisbeck, S. Sequeira, F. Yiou, and K. Mork (2004), Correction to 'The
 461 Norwegian Atlantic Current in the Lofoten basin inferred from hydrological and tracer
 462 data(I-129) and its interaction with the Norwegian Coastal Current'. *Geophys. Res.*
 463 *Lett.*, 31(8), doi: 10.1029/2003GL018303.
- 464 Gascard, J. C., G. Raisbeck, S. Sequeira, F. Yiou, and K. Mork (2004), Correction to
 465 2003GL01803, *Geophys. Res. Lett.*, 31, L08302, doi:10.1029/2004GL020006, 2004.
- 466 Gevirtz, J. L., and G. M. Friedman (1966), Deep-Sea carbonate sediments of the Red Sea and
 467 their implications on marine lithification, *J. Sed. Petrol.*, 36, 143-151.
- 468 Gruber, N., and J. L. Sarmiento (1997), Global patterns of marine nitrogen fixation and
 469 denitrification, *Global Biogeochem. Cycles*, 11(2), 235-266, doi: 10.1029/97GB00077.
- 470 Hales, B. (2003), Respiration, dissolution, and the lysocline. *Paleoceanogr.*, 18(4), 1099, doi:
 471 10.1029/2003PA000915.
- 472 Hales, B., and S. Emerson (1997), Calcite dissolution in sediments of the Ceara Rise: In situ
 473 measurements of porewater O₂, pH, and CO₂ (aq). *Geochim. Cosmochim. Acta*, 61(3), 501-
 474 514, doi:10.1016/S0016-7037(96)00366-3.

Formatted: Subscript

Formatted: Subscript

- 475 Honjo, S., S. J. Manganini, R. A. Krishfield, and R. Francois (2008), Particulate organic carbon
476 fluxes to the ocean interior and factors controlling the biological pump: A synthesis of global
477 sediment trap programs since 1983, *Prog. Oceanogr.*, 76(3), 217-285,
478 [doi:10.1016/j.pocean.2007.11.003](https://doi.org/10.1016/j.pocean.2007.11.003).
- 479 Ilyina, T. R. E. Zeebe, E. Maier-Reimer, and C. Heinze (2009), Early detection of ocean
480 acidification effects on marine calcification, *Global Biogeochem. Cycles*, 23, GB1008, doi:
481 10.1029/2008GB003278.
- 482 Jiang, Z. P., T. Tyrrell, D.J. Hydes, M. Dai, and S.E. Hartman (2014), Variability of alkalinity
483 and the alkalinity-salinity relationship in the tropical and subtropical surface ocean. *Global*
484 *Biogeochem. Cycles*, 28(7), 729-742, doi: 10.1002/2013GB004678.
- 485 Jones, E. P., L. G. Anderson, S. Jutterström, L. Mintrop, and J. H. Swift (2008), Pacific
486 freshwater, river water and sea ice meltwater across Arctic Ocean basins: Results from the
487 2005 Beringia Expedition, *J. Geophys. Res. Oceans*, 113(C8), [doi: 10.1029/2007JC004124](https://doi.org/10.1029/2007JC004124).
- 488 Kanamori, S. and H. Ikegami (1982), Calcium-alkalinity relationship in the North Pacific, *J.*
489 *Oceanogr.*, 38, 57-62, [doi: 10.1007/BF02110291](https://doi.org/10.1007/BF02110291).
- 490 Kaushal, S. S., G. E. Likens, R. M. Utz, M. L. Pace, M. Grese, and M. Yepsen (2013), Increased
491 river alkalization in the Eastern U.S., *Envi. Sci. Tech.*, 47, 10302-10311, doi:
492 10.1021/es401046s.
- 493 Key, R. M., A. Kozyr, C. L. Sabine, K. Lee, R. Wanninkhof, J. L. Bullister, R. A. Feely, F. J.
494 Millero, C. Mordy, and T. H. Peng (2004), A global ocean carbon climatology: Results from
495 Global Data Analysis Project (GLODAP), *Global Biogeochem. Cycles*, 18, GB4031, doi:
496 10.1029/2004GB002247.
- 497 Key, R. M., T. Tanhua, A. Olsen, M. Hoppema, S. Jutterström, C. Schirnick, S. van Heuven, X.

- 498 Lin, D. Wallace and L. Mintrop (2009), The CARINA data synthesis project: Introduction
 499 and overview, *Earth Sys. Sci. Data*, 2(1), 579-624, [doi:10.5194/essdd-2-579-2009](https://doi.org/10.5194/essdd-2-579-2009).
- 500 Khatiwala, S., M. Visbeck, and M. A. Cane, (2005), Accelerated simulation of passive tracers in
 501 ocean circulation models, *Ocean Modelling*, 9(1), 51-69, [doi:10.1016/j.ocemod.2004.04.002](https://doi.org/10.1016/j.ocemod.2004.04.002).
- 502 Khatiwala, S. (2007), A computational framework for simulation of biogeochemical tracers in
 503 the ocean, *Global Biogeochemical Cycles*, 21(3), GB3001, [doi: 10.1029/2007GB002923](https://doi.org/10.1029/2007GB002923).
- 504 Mehrbach, C., C. H. Culbertson, J. E. Hawley, and R. M. Pytkowicz (1973), Measurement of the
 505 apparent dissociation constants of carbonic acid in seawater at atmospheric pressure, *Limnol.*
 506 *Oceanogr.*, 18, 897-907.
- 507 Millero, F. J., K. Lee, and M. Roche, (1998), Distribution of alkalinity in the surface waters of
 508 the major oceans, *Marine Chemistry*, 60, 111-130, [doi:10.1016/S0304-4203\(97\)00084-4](https://doi.org/10.1016/S0304-4203(97)00084-4).
- 509 Milliman, J. D., D. A. Ross, and T. L. Ku (1969), Precipitation and lithification of deep-sea
 510 carbonates in the Red Sea, *J. Sed Res.*, 39(2), 724-736, [doi: 10.1306/74D71CFD-2B21-](https://doi.org/10.1306/74D71CFD-2B21-11D7-8648000102C1865D)
 511 [11D7-8648000102C1865D](https://doi.org/10.1306/74D71CFD-2B21-11D7-8648000102C1865D).
- 512 [Morse, J. W., A. J. Andersson, F. T. Mackenzie \(2006\), Initial responses of carbonate-rich shelf](#)
 513 [sediments to rising atmospheric pCO₂ and “ocean acidification”: Role of high Mg-calcites.](#)
 514 [Geochim. Cosmochm. Acta., 70 \(23\), 5814-5830, doi:10.1016/j.gca.2006.08.017.](#)
- 515 Moore, W. S. (2010), The effect of submarine groundwater discharge on the ocean. *Marine Sci.*,
 516 2, 59-88, doi: 10.1146/annurev-marine-120308-081019
- 517 Moore, W. S., J. L. Sarmiento, and R. M. Key (1986), Tracing the Amazon component of surface
 518 Atlantic water using ²²⁸Ra, salinity, and silica, *J. Geophys. Res.*, 91 (C2), 2574-2580,
 519 [doi: 10.1029/JC091iC02p02574](https://doi.org/10.1029/JC091iC02p02574).
- 520 [Orr, J. C., V. J. Fabry, O. Aumont, L. Bopp, S. C. Doney, R. A. Feely, A. Gnanadesikan, N.](#)

Formatted: Font: Not Bold

- 521 [Gruber, A. Ishida, F. Joos, R. M. Key, K. Lindsay, E. Maier-Reimer, R. Matear, P. Monfray,](#)
 522 [A. Mouchet, R. G. Najjar, G. Plattner, K. B. Rodgers, C. L. Sabine, J. L Sarmiento, R.](#)
 523 [Schlitzer, R. D. Slater, I. J. Totterdell, M. Weirig, Y. Yamanaka, and A. Yool, \(2005\),](#)
 524 [Anthropogenic ocean acidification over the twenty-first century and its impact on calcifying](#)
 525 [organisms. *Nature*, 437, 681-686, doi:10.1038/nature04095.](#)
- 526 Robbins, P. E. (2001), Oceanic carbon transport carried by freshwater divergence: Are salinity
 527 normalizations useful?. *J. Geophys. Res*, 106(C12), 30939-30, doi: 10.1029/2000JC000451.
- 528 Sarmiento, J. L., J. Dunne, A. Gnanadesikan, R.M. Key, K. Matsumoto, R. Slater (2002), A new
 529 estimate of the CaCO₃ to organic carbon export ratio. *Global Biogeochem. Cy.*, 16(4), 1107,
 530 doi: 10.1029/2002GB001919.-
- 531 Sarmiento, J. L., N. Gruber, M. A. Brzezinski, and J. P. Dunne (2004), High-latitude controls of
 532 thermocline nutrients and low latitude biological productivity. *Nature*, 427(6969), 56-60,
 533 doi:10.1038/nature02127.-
- 534 Silverman, J. B. Lazar, and J. Erez (2007), Effect of aragonite saturation, temperature, and
 535 nutrients on the community calcification rate of a coral reef, *J. Geophys. Res.*, 112,
 536 CO05004, DOI: 10.1029/2006JC003770.
- 537 Suzuki, T., M. Ishii, M. Aoyama, J. R. Christian, K. Enyo, T. Kawano, R. M. Key, N. Kosugi, A.
 538 Kozyr, L. A. Miller, A. Murata, T. Nakano, T. Ono, T. Saino, K. Sasaki, D. Sasano, Y.
 539 Takatani, M. Wakita and C. Sabine (2013), PACIFICA Data Synthesis Project.
 540 ORNL/CDIAC-159, NDP-092. Carbon Dioxide Information Analysis Center, Oak Ridge
 541 National Laboratory, U.S. Department of Energy, Oak Ridge, Tennessee.
 542 doi:10.3334/CDIAC/OTG.PACIFICA_NDP092.
- 543 Takahashi, T., S. C. Sutherland, R. Wanninkhof, C. Sweeney, R. A. Feely, D. W. Chipman, B.

Formatted: Subscript

544 Hales, G. Friederich, F. Chavez, C. Sabine, A. Watson, D. C. E. Bakker, U. Schuster, N.
545 Metzl, H. Yoshikawa-Inoue, M. Ishii, T. Midorikawa, Y. Nojiri, A. Körtzinger, T. Steinhoff,
546 M. Hoppema, J. Olafsson, T. S. Arnarson, B. Tilbrook, T. Johannessen, A. Olsen, R.
547 Bellerby, C. S. Wong, B. Delille, N. R. Bates, and J. W. deBarr, (2009), Climatological mean
548 and decadal change in surface ocean pCO₂, and net sea–air CO₂ flux over the global
549 oceans, *Deep Sea Res. II*, 56(8), 554-577, [doi:10.1016/j.dsr2.2008.12.009](https://doi.org/10.1016/j.dsr2.2008.12.009).
550 Thomas, H., Y. Bozec, H. J. De Baar, K. Elkalay, M. Frankignoulle, L. S. Schiettecatte, G.
551 Kattner, and A. V. Borges (2005), The carbon budget of the North Sea. *Biogeosci.*, 2(1), 87-
552 96, [doi: 10.5194/bg-2-87-2005](https://doi.org/10.5194/bg-2-87-2005).
553 Tynan, E., T. Tyrrell, and E. P. Achterberg (2014), Controls on the seasonal variability of
554 calcium carbonate saturation states in the Atlantic gateway to the Arctic Ocean. *Mar. Chem.*
555 158 (2014) 1-9, [doi: 10.1016/j.marchem.2013.10.010](https://doi.org/10.1016/j.marchem.2013.10.010).
556 van Heuven, S., D. Pierrot, E. Lewis, and D. Wallace (2009), MATLAB Program developed for
557 CO₂ system calculations, *ORNL/CDIAC-105b, Carbon Dioxide Information Analysis Center,*
558 *Oak Ridge National Laboratory, US Department of Energy, Oak Ridge, Tennessee.*
559 Velo, A., F. F. Perez, P. Brown, T. Tanhua, U. Schuster, and R. M. Key (2009), CARINA
560 alkalinity data in the Atlantic Ocean, *Earth Syst. Sci. Data*, 1, 45-61, doi:10.5194/essd-1-45-
561 2009.
562 de Villiers, S. (1998), Excess dissolved calcium in the ocean: a hydrothermal hypothesis, *Earth*
563 *and Plan. Sci. Lett.*, 164(3-4), 624-641, [doi:10.1016/S0012-821X\(98\)00232-5](https://doi.org/10.1016/S0012-821X(98)00232-5).
564 Wolery, T. J., and N. H. Sleep (1988), Interactions of geochemical cycles with the mantle. In:
565 Gregor, C. B., R. M. Garrels, F. T. Mackenzie, and J. B. Maynard (eds) *Chemical cycles in*
566 *the evolution of the earth.* Wiley, New York, 77-103.

567 Wolf-Gladrow, D. A., R. E. Zeebe, C. Klaas, A. Körtzinger, and A. G. Dickson (2007), Total
568 alkalinity: The explicit conservative expression and its application to biogeochemical
569 processes. *Marine chemistry*, 106(1), 287-300, [doi:10.1016/j.marchem.2007.01.006](https://doi.org/10.1016/j.marchem.2007.01.006).

570 Yamamoto-Kawai, M., F. A. McLaughlin, E. C. Carmack, S. Nishino, and K. Shimada (2009),
571 Aragonite undersaturation in the Arctic Ocean; effects of ocean acidification and sea ice
572 melt, *Science*, 326, 1098, doi:10.1126/science.1174190.

573 **Appendix A: Definition of the process importance metric M**

574 In simplest terms, our metric is the product of the Ω_C calcite saturation sensitivity to a
 575 process and the variability of the net influence of the process globally. The difficulty in this
 576 calculation lies in quantifying the “net influence of a process.” We first show how we change
 577 coordinates so we can use reference tracers as a proxy measurement for these net influences.

578 Our metric for Ω_C variability resulting from the i th process is expressed as M_i :

$$579 \quad M_i = \sigma_{P_i} \left| \frac{\partial \Omega_C}{\partial P_i} \right| \quad (\text{A1})$$

580 where P_i is an abstract variable representing the net process influence (that we will later factor
 581 out), and $\frac{\partial \Omega_C}{\partial P_i}$ is the Ω_C calcite saturation sensitivity to the process. We expand $\frac{\partial \Omega_C}{\partial P_i}$ using the
 582 chain rule to include a term for Ω_C sensitivity to changes in the reference tracer R_i (see section 4)
 583 and a term $\frac{\partial R_i}{\partial P_i}$ representing changes in R_i resulting from the i th process:

$$584 \quad \frac{\partial \Omega_C}{\partial P_i} = \frac{\partial \Omega_C}{\partial R_i} \frac{\partial R_i}{\partial P_i} \quad (\text{A2})$$

585 In practice, we calculate Ω_C as a function of $j = 7$ properties: (1) pressure, (2)
 586 temperature, (3) salinity, (4) phosphate, (5) silicate, (6) A_T , and (7) C_T for mean seawater and
 587 $p\text{CO}_2$ for surface seawater, so we use the chain rule again to expand the $\frac{\partial \Omega_C}{\partial R_i}$ terms as follows:

$$588 \quad \frac{\partial \Omega_C}{\partial R_i} = \sum_{j=1}^7 \frac{\partial \Omega_C}{\partial X_j} \frac{\partial X_{j,i}}{\partial R_i} \quad (\text{A3})$$

589 Here, the $\frac{\partial X_{j,i}}{\partial R_i}$ are assumed terms (assumptions detailed shortly) that relate the effect of the i th

Field Code Changed

Field Code Changed

590 process on the j th property to the effect of the process on R_i , and the $\frac{\partial\Omega}{\partial X_j}$ terms reflect Ω_c ~~calculate~~
 591 ~~saturation~~ sensitivity to changes in the j properties used to calculate it.

592 We make assumptions regarding the $\frac{\partial X_{j,i}}{\partial X_R}$ terms: we relate changes in temperature from
 593 sinking or shoaling to changes in pressure using the potential temperature (θ) routines of
 594 Fofonoff and Millard (1983); we assume freshwater cycling linearly concentrates A_T , C_T ,
 595 phosphate, and silicate by the same ratio that it changes salinity; we relate C_T , phosphate, and A_T
 596 changes from organic matter formation to changes in phosphate using the remineralization ratios
 597 found by Anderson and Sarmiento (1994) and the empirical relationship of Kanamori and
 598 Ikegami (1982); we also use Kanamori and Ikegami (1982)'s constant to relate changes in A_T
 599 from nitrogen fixation and denitrification to changes in N^* from these processes; and we assume
 600 that an increase in A_T from calcium carbonate dissolution equals the Alk^* increase, and that the
 601 corresponding increase in C_T equals half of this Alk^* increase. We neglect any changes in C_T
 602 from denitrification and nitrogen fixation because these changes are better thought of as organic
 603 matter cycling occurring alongside nitrogen cycling.

604 We estimate $\frac{\partial\Omega}{\partial X_j}$ property sensitivity terms as the differences between Ω_c calculated
 605 before and after augmenting j th property by 1 unit. Ω_c is calculated with the MATLAB
 606 CO2SYS routines written by van Heuven et al. (2009) using the carbonate system equilibrium
 607 constants of Mehrbach et al. (1973), as refit by Dickson and Millero (1987). Seawater pCO_2 is
 608 used in place of C_T for the surface seawater calculations (when $j = 7$) to calculate the change in
 609 Ω_c that remains after the surface seawater is allowed to equilibrate with the atmosphere.

Field Code Changed

610 We assume that the distributions of our R_i reference properties are linearly related to the
 611 P_i net activities of their associated processes. This assumption implies:

$$612 \quad \sigma_p = \sigma_{R_i} \left| \frac{\partial P_i}{\partial R_i} \right| \quad (\text{A4})$$

613 We can then substitute Eq. (A3) into Eq. (A2), and substitute this combined equation for $\frac{\partial \Omega_C}{\partial P_i}$

614 and (A4) into Eq. (A1). We then ~~and~~ cancel the $\frac{\partial P_i}{\partial R_i}$ and $\frac{\partial R_i}{\partial P_i}$ terms to obtain:

$$615 \quad M_i = \sigma_{R_i} \left| \sum_{j=1}^7 \frac{\partial \Omega_C}{\partial X_j} \frac{\partial X_{j,i}}{\partial R_i} \right| \quad (\text{A5})$$

616 We then define ~~our Ω_C saturation~~ sensitivity S_{R_i} as:

$$617 \quad S_{R_i} = \left| \sum_{j=1}^7 \frac{\partial \Omega_C}{\partial X_j} \frac{\partial X_{j,i}}{\partial R_i} \right| \quad (\text{A6})$$

618 where S_{R_i} is the ~~Ω_C saturation~~ sensitivity to a change in the i th process scaled to a unit change in
 619 the reference variable for that process. We can then substitute Eq. (A6) into Eq. (A5) to obtain

620 Eq. 6. We use Eqn. (A6) to define S_{R_i} and Eqn. 6 to calculate M . We provide the $\frac{\partial \Omega_C}{\partial X_j}$ and

621 $\frac{\partial X_{j,i}}{\partial R_i}$ values we use to estimate S_{R_i} for atmospherically isolated seawater from all depths in

622 Table A1 and for well-equilibrated surface seawater in Table A3. We perform a sample I and M
 623 calculation in Supplementary Materials document SE.

624 We use a Monte Carlo analysis to estimate variability and uncertainty in our metric M
 625 and our percent relative process importance I calculations. We calculate the standard deviations,
 626 σ_M and σ_I , of pools of 1000 M and I estimates calculated after adjusting the seawater properties

Field Code Changed

Field Code Changed

627 X_i with a normally-distributed perturbation with a standard deviation equal to the property

628 standard deviation from the gridded dataset. We find $\frac{\sigma_I}{I}$ is typically much smaller than $\frac{\sigma_M}{M}$.

629 This is because Ω_c ~~calcite saturation~~ sensitivity is typically proportional to the Ω_c ~~calcite~~

630 ~~saturation~~ itself, so individual Monte Carlo M estimates vary with the initial Ω_c ~~initial calcite~~

631 ~~saturation~~ and one another. Our σ_M estimates are therefore better thought of as measures of the

632 ranges of sensitivities found in the modern ocean, while σ_I represent variability in the relative

633 importance of processes. We provide σ_M and σ_I for atmospherically isolated seawater globally

634 in Table A2, and for well-equilibrated surface seawater in Table A4.

635

636

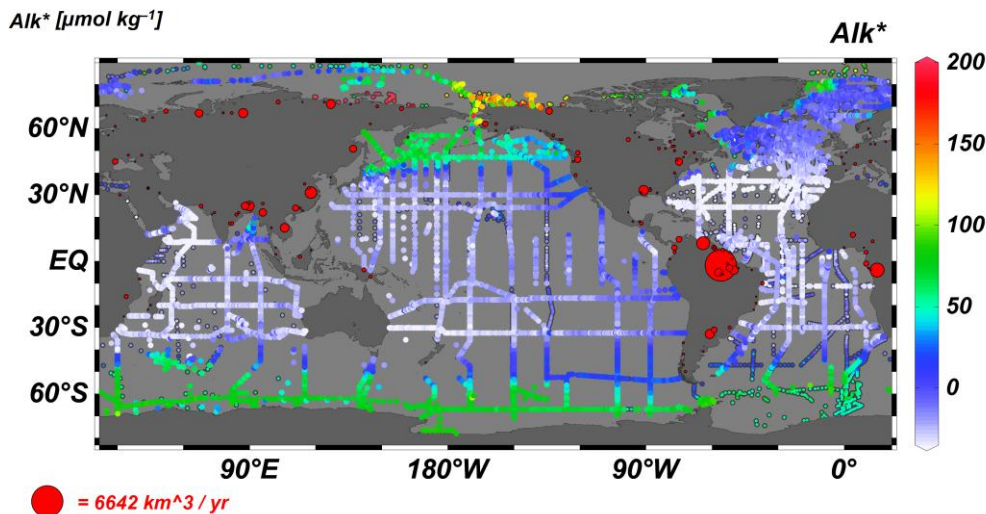


Figure 1. A map of station locations at which we use measurements to estimate Alk^* (in $\mu\text{mol kg}^{-1}$). Dot color indicates surface Alk^* . Points with black borders indicate that either A_T was measured prior to 1992 (i.e. before reference materials were commonly used) or that no nitrate value was reported (in which case a nitrate concentration of $5 \mu\text{mol kg}^{-1}$ is assumed). Red dots on land indicate the mouth locations and mean annual discharge volumes (indicated by dot size) of 200 large rivers, as given by Dai and Trenberth (2002).

Field Code Changed

Field Code Changed

Field Code Changed

637

638

639

640

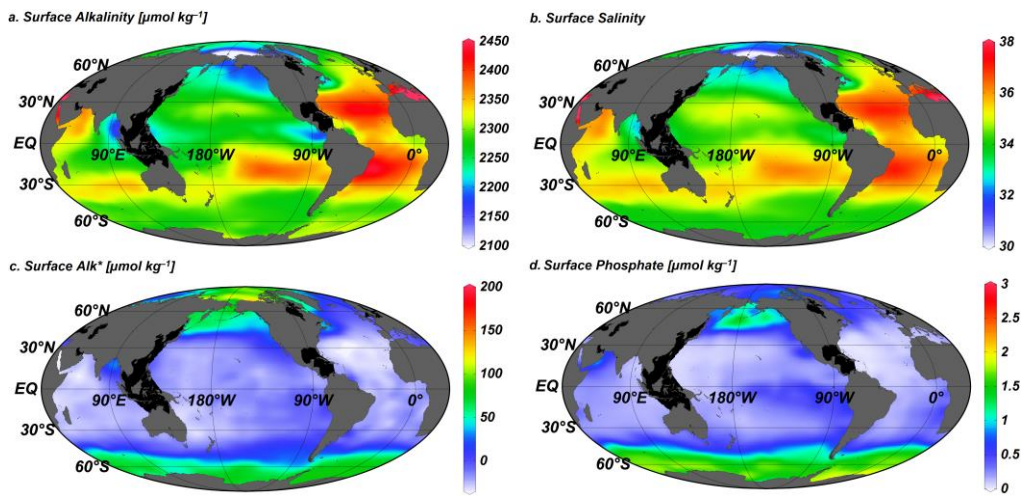


Figure 2. Global (a) total alkalinity A_T , (b) salinity, (c) Alk^* , and (d) phosphate distributions at the surface (10 m depth surface) from our gridded CARINA, PACIFICA, and GLODAP bottle data product [detailed in Supplementary Materials document SA](#). Areas with exceptionally poor coverage in the data used to produce the gridded product are blacked out.

641

642

643

644

645

646

647

648

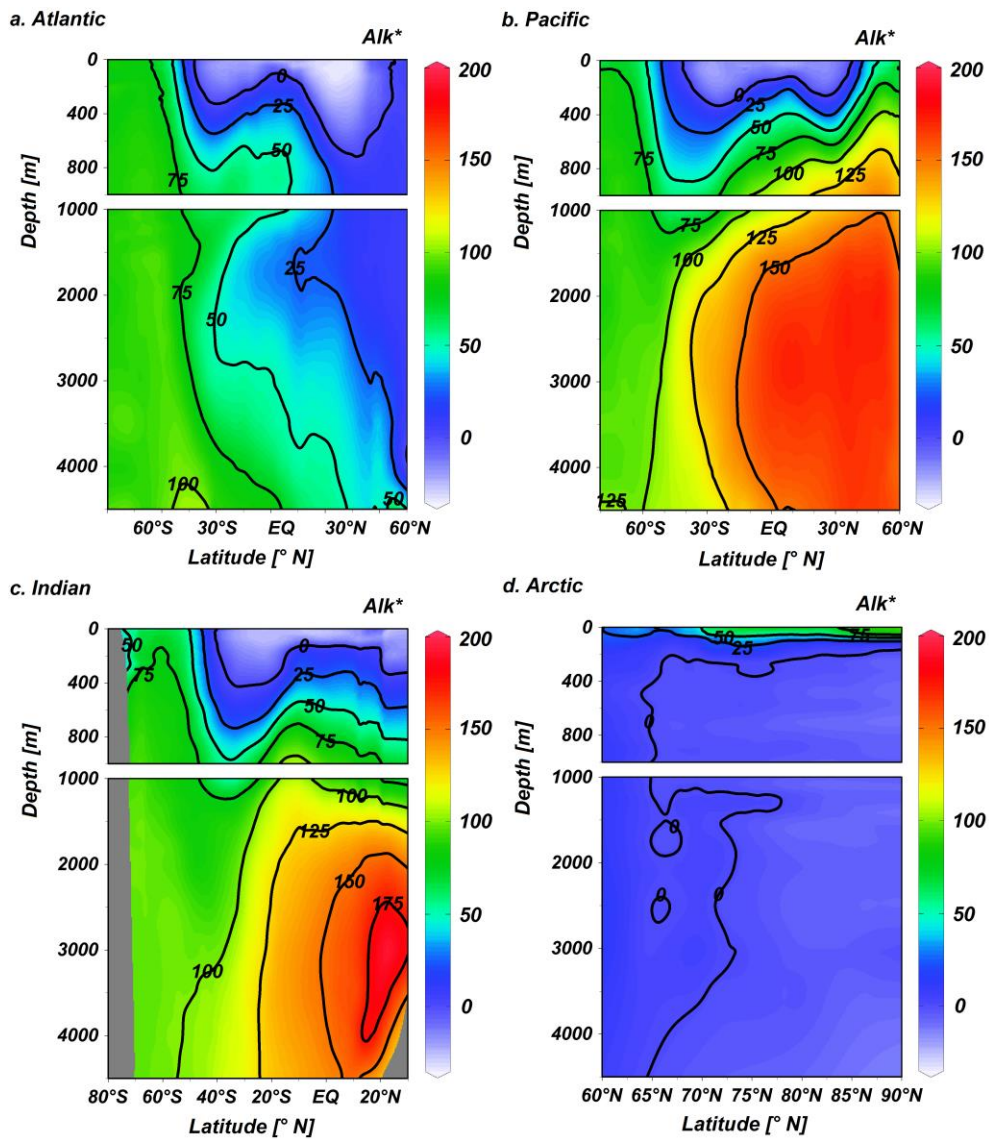


Figure 3. Zonal mean gridded Alk^* (in $\mu\text{mol kg}^{-1}$) in the (a) Atlantic, (b) Pacific, (c) Indian, and (d) the Arctic oceans plotted against latitude and depth.

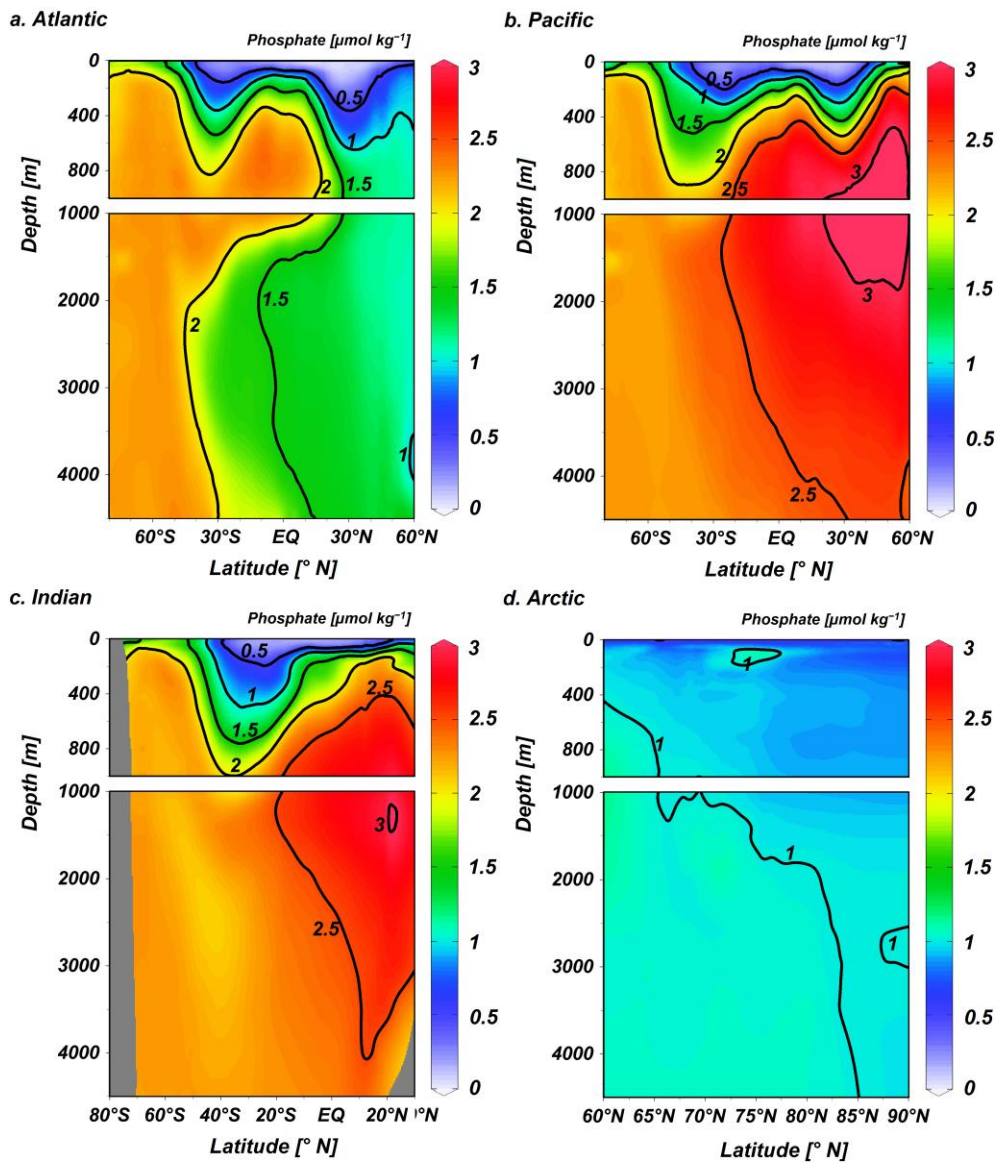


Figure 4. Zonal mean gridded phosphate (in $\mu\text{mol kg}^{-1}$) in the (a) Atlantic, (b) Pacific, (c) Indian, and (d) the Arctic oceans plotted against latitude and depth.

650

651

652

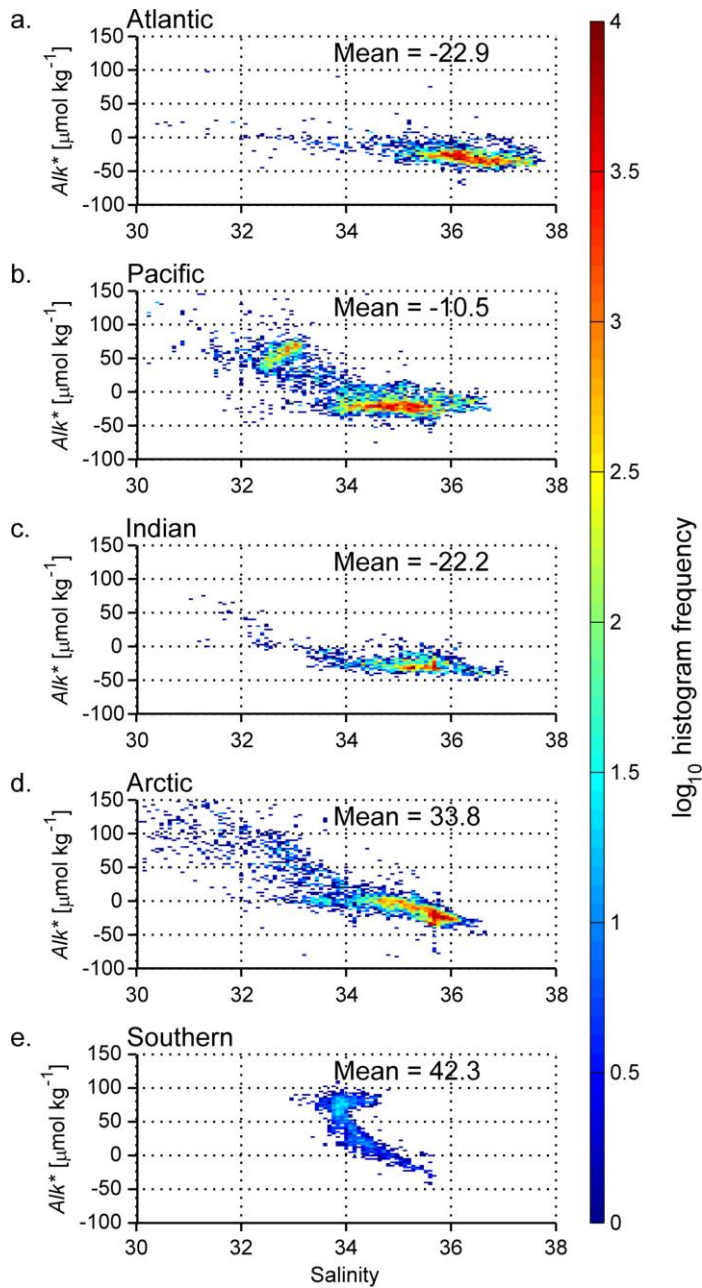


Figure 5. 2-D histograms indicating the log (base 10) of the number of measurements that fall within bins of Alk^* vs. salinity with color. Data are limited to the top 50 m of the (a) Atlantic, (b) Pacific, (c) Indian, (d) Arctic, and (e) Southern Oceans. Where basins connect, the boundary between the Atlantic and the Arctic oceans is 40°N , between the Atlantic and the Indian is 20°E ,

between the Indian and the Pacific is 131° E, between the Pacific and the Atlantic is 70° W, and between the Southern Ocean and the other oceans is 40° S.

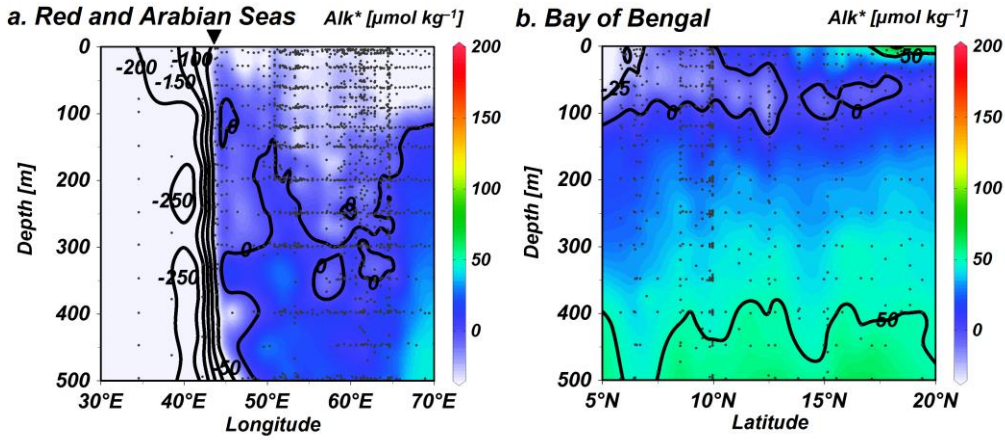


Figure 76. Alk^* distributions (in $\mu\text{mol kg}^{-1}$) (a) between 5° and 30°N in the Red and Arabian Seas shown against longitude, and (b) between 75° and 100° E in the Bay of Bengal plotted against latitude. Small black dots indicate where data is present. The inverted triangle above (a) indicates the longitude of the mouth of the Red Sea.

654

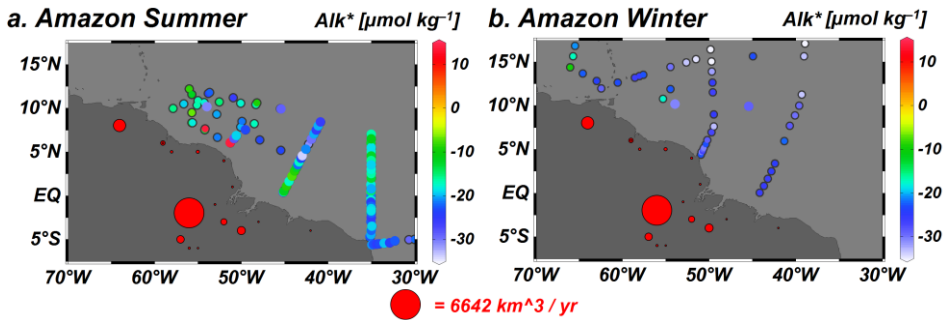


Figure 67. Alk^* (in $\mu\text{mol kg}^{-1}$) in top 50 m of the ocean near the Amazon River outflow plotted in color, though with a narrower color scale than is used for all other plots. Panel (a) is limited to data collected in November through January, and in panel (b) is limited to measurements from May through July. Points with black borders indicate that either the A_T was measured prior to 1992 (before reference materials were commonly used) or that no nitrate value was reported (in which case a nitrate concentration of $5 \mu\text{mol kg}^{-1}$ is assumed). Red dots on land indicate the mouth locations and mean annual discharge volumes (indicated by dot size) of large rivers, as given by Dai and Trenberth (2002).

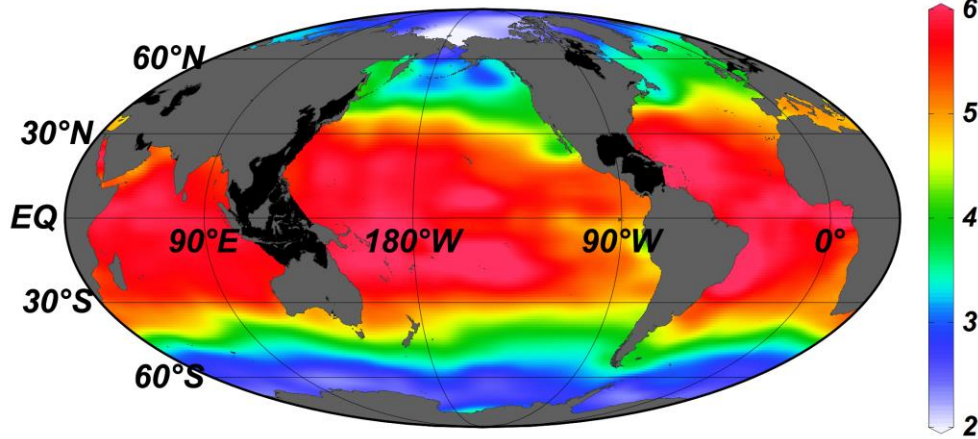
655

656

657

658

a. Surface Calcite Saturation



b. Surface Temperature [$^{\circ}\text{C}$]

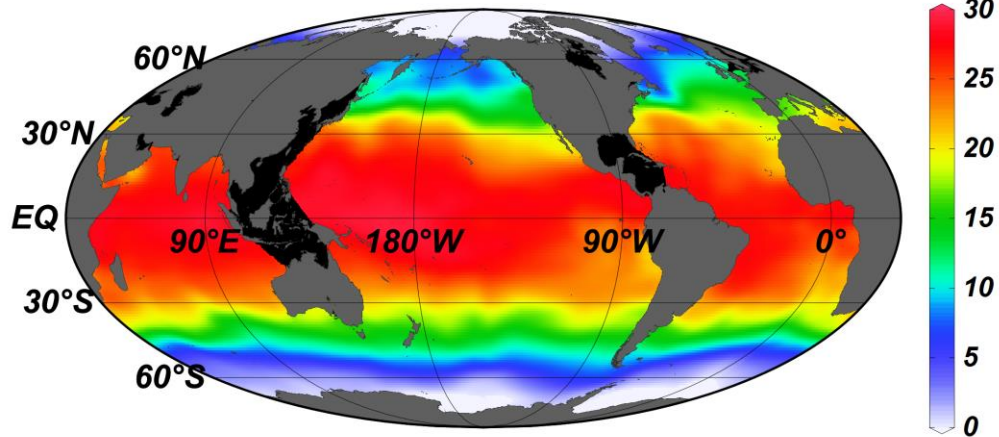


Figure 8. Gridded global (a) calcite saturation state Ω_c , and (b) temperature at the surface (10 m depth surface) of our gridded CARINA, PACIFICA, and GLODAP bottle data product. Areas with exceptionally poor coverage in the data used to produce the gridded product are blacked out.

Field Code Changed

659

660

661

662

663

664

Table 1. Metric estimates M_i , relative process importance percentages I_i , Ω_C ~~calcite saturation~~ sensitivities S_{R_i} to unit changes in the R_i reference properties, and reference property standard deviations σ_{R_i} for the $i = 6$ processes in atmospherically isolated mean seawater from all ocean depths. See Appendix A for details on how these terms are estimated and explanation of how M_i and I_i uncertainties are obtained.

Field Code Changed

Process	i	R_i	S_{R_i}	σ_{R_i}	M_i	I_i
Carbonate cycling	1	Alk^*	0.0043	53.5 $\mu\text{mol/kg}$	0.23	17%
Org. matter cycling	2	Phosphate	-0.0069	0.60 $\mu\text{mol/kg}$	0.66	48%
Freshwater cycling	3	Salinity	0.032	0.27	0.011	0.78%
Sinking / shoaling	4	Pressure	-0.00028	1411 db	0.4	28%
Warming / cooling	5	Temp.	0.014	4.20 $^{\circ}\text{C}$	0.06	4%
Denit./nit. fix.	6	N^*	-0.010	1.6 $\mu\text{mol/kg}$	0.017	1.2%

665

666

Table 2. Metric estimates M_i , relative process importance percentages I_i , Ω_C ~~calcite saturation~~ sensitivities S_{R_i} to unit changes in the R_i reference properties, and reference property standard deviations σ_{R_i} for the $i = 6$ processes in well-equilibrated surface seawater. See Appendix A for details on how these terms are estimated and explanation of how M_i and I_i uncertainties are obtained.

Field Code Changed

Process	i	R_i	S_{R_i}	σ_{R_i}	M_i	I_i
Carbonate cycling	1	Alk^*	0.0034	36.9 $\mu\text{mol/kg}$	0.13	7.8%
Org. matter cycling	2	Phosphate	-0.0045	0.51 $\mu\text{mol/kg}$	0.037	2.3%
Freshwater cycling	3	Salinity	0.20	0.86	0.22	13.2%
Sinking / shoaling	4	Pressure	-0.00083	15 db	0.011	0.70%
Warming / cooling	5	Temp.	0.14	8.8 $^{\circ}\text{C}$	1.2	76%
Denit. / nit. fix.	6	N^*	-0.0043	1.5 $\mu\text{mol/kg}$	0.006	0.40%
$p\text{CO}_2$ disequilibria	†	$p\text{CO}_2$	-0.0086	27 μatm^*	0.23	†

* standard deviation of the Takahashi et al. (2009) revised global monthly $p\text{CO}_2$ climatology

† the M value for disequilibria is only calculated to test our assumption of surface seawater air-sea equilibration, and is omitted from calculations of I_i for comparison with Table 1.

669

670

Table A1. $\frac{\partial \Omega_c}{\partial X_j}$ (bold text) and $\frac{\partial X_{j,i}}{\partial R_i}$ (italic text) terms used in Eq. (A5) for atmospherically isolated mean seawater from all ocean depths. These terms are specific to the $j = 7$ (columns) properties we use to calculate Ω_c and $i = 6$ (rows) processes we consider. Units for $\frac{\partial \Omega_c}{\partial X_j}$ are the inverse of the listed X_j units. Units for $\frac{\partial X_{j,i}}{\partial R_i}$ are the X_j units divided by the R_i units

given in Table 1.

<i>Properties</i>	Pressure	Temp	Salinity	Phos.	Silicate	A_T	C_T	
<i>X_j units</i>	db	$^{\circ}\text{C}$		$\mu\text{mol/kg}$	$\mu\text{mol/kg}$	$\mu\text{mol/kg}$	$\mu\text{mol/kg}$	
<i>j</i>	1	2	3	4	5	6	7	
<i>Mean seawater values</i>	2235	3.7	34.71	2.15	49.0	2362	2254	
$\frac{\partial \Omega_c}{\partial X_j}$	-0.00028	0.014	-0.011	-0.0085	-0.00012	0.0082	-0.0079	
Process	<i>i</i>	$\frac{\partial X_{1,i}}{\partial R_i}$	$\frac{\partial X_{2,i}}{\partial R_i}$	$\frac{\partial X_{3,i}}{\partial R_i}$	$\frac{\partial X_{4,i}}{\partial R_i}$	$\frac{\partial X_{5,i}}{\partial R_i}$	$\frac{\partial X_{6,i}}{\partial R_i}$	$\frac{\partial X_{7,i}}{\partial R_i}$
Carbonate cycling	1	-	-	-	-	-	<i>1</i>	<i>0.5</i>
Org. matter cycling	2	-	-	-	<i>1</i>	-	<i>-20.16</i>	<i>117</i>
Freshwater cycling	3	-	-	<i>1</i>	<i>0.062</i>	<i>1.4</i>	<i>68</i>	<i>65</i>
Sinking / shoaling	4	<i>1</i>	<i>0.00010</i>	-	-	-	-	-
Warming / cooling	5	-	<i>1</i>	-	-	-	-	-
Denit. / nit. fix.	6	-	-	-	-	-	<i>-1.26</i>	-

Field Code Changed

Field Code Changed

Field Code Changed

Field Code Changed

Field Code Changed

Field Code Changed

671

672

673

674

Table A2. Monte Carlo derived estimates for M_i variability (σ_{M_i}) and I_i variability (σ_{I_i}) for atmospherically-isolated mean seawater from all ocean depths.

Process	i	σ_{M_i}	σ_{I_i}
Carbonate cycling	1	0.09	1%
Org. matter cycling	2	0.2	3%
Freshwater cycling	3	0.006	0.08%
Sinking / shoaling	4	0.2	5%
Warming / cooling	5	0.02	2%
Denit. / nit. fix.	6	0.006	0.1%

675

676

677

Table A3. $\frac{\partial \Omega_c}{\partial X_j}$ (bold text) and $\frac{\partial X_{j,i}}{\partial R_i}$ (italic text) terms used in Eq. (A5) for well-equilibrated surface seawater. These terms are specific to the $j = 7$ (columns) properties we use to calculate Ω_c and $i = 6$ (rows) processes we consider. Units for $\frac{\partial \Omega_c}{\partial X_j}$ are the inverse of the listed X_j units. Units for $\frac{\partial X_{j,i}}{\partial R_i}$ are the X_j units divided by the R_i units given in Table 2.

<i>Properties</i>		Pressure	Temp	Salinity	Phos.	Silicate	A_T	$p\text{CO}_2$
<i>units</i>		db	°C		$\mu\text{mol/kg}$	$\mu\text{mol/kg}$	$\mu\text{mol/kg}$	μatm
<i>j</i>		1	2	3	4	5	6	7
<i>Mean seawater values</i>		25	18.3	34.82	0.51	2.5	2305	350
$\frac{\partial \Omega_c}{\partial X_j}$		-0.00084	0.14	-0.022	-0.0038	-0.00013	0.0034	-0.0086
<i>Process</i>	<i>i</i>	$\frac{\partial X_{1,i}}{\partial R_i}$	$\frac{\partial X_{2,i}}{\partial R_i}$	$\frac{\partial X_{3,i}}{\partial R_i}$	$\frac{\partial X_{4,i}}{\partial R_i}$	$\frac{\partial X_{5,i}}{\partial R_i}$	$\frac{\partial X_{6,i}}{\partial R_i}$	$\frac{\partial X_{7,i}}{\partial R_i}$
Carbonate cycling	1	-	-	-	-	-	1	-
Org. matter cycling	2	-	-	-	1	-	-20.16	-
Freshwater cycling	3	-	-	1	0.015	0.072	65.9	-
Sinking / shoaling	4	1	0.00010	-	-	-	-	-
Warming / cooling	5	-	1	-	-	-	-	-
Denit./nit. fix.	6	-	-	-	-	-	-1.26	-

678

679

Table A4. Monte Carlo derived estimates for M_i variability (σ_{M_i}) and I_i variability (σ_{I_i}) for well-equilibrated surface seawater.

Process	i	σ_{M_i}	σ_{I_i}
Carbonate cycling	1	0.03	0.8%
Org. matter cycling	2	0.01	0.2%
Freshwater cycling	3	0.04	0.5%
Sinking / shoaling	4	0.001	0.03%
Warming / cooling	5	0.2	1%
Denit. / nit. fix	6	0.002	0.04%
$p\text{CO}_2$ disequilibria	†	0.05	†

† disequilibria are included only as a test of our assumption of surface seawater air-sea equilibration, so these M_i values are omitted from calculations of I

680

681

682